THESIS

EXPERIMENTAL AND NUMERICAL PERFORMANCE EVALUATION OF A THERMAL OXIDIZER FOR INDUSTRIAL LEAN BURN NATURAL GAS ENGINES

Submitted by

Andrew Joseph Huonder

Department of Mechanical Engineering

In partial fulfillment of the requirements

For the Degree of Master of Science

Colorado State University

Fort Collins, Colorado

Spring 2025

Master's Committee:

Advisor: Daniel Olsen

Bret Windom
Joe von Fischer

ABSTRACT

EXPERIMENTAL AND NUMERICAL PERFORMANCE EVALUATION OF A THERMAL OXIDIZER FOR INDUSTRIAL LEAN BURN NATURAL GAS ENGINES

Methane slip in industrial lean burn natural gas engines is a significant source of greenhouse gas emissions. With growing regulations on the emissions of hydrocarbon pollutants, especially methane, new reduction technologies for these engines are needed. This research investigates the performance of a new type of thermal oxidizer, known as an Oxiperator, for reducing methane emissions from a lean burn natural gas engine. This study begins with baseline testing of a Cummins QSK19G engine to determine the optimal operating conditions for the Oxiperator. It was found that the most optimal operating condition for the Oxiperator is with a high air-to-fuel mixture. It was then followed by a performance evaluation of the Oxiperator to assess its ability to oxidize methane in the exhaust. The first key result from this performance evaluation is that the minimum concentration of total hydrocarbons required to maintain oxidation was found to be 4400 ppm. The second key result was that the lowest temperature that the Oxiperator can be where the oxidation reaction is still recoverable is 815 °C. The performance of the Oxiperator was also modeled using CONVERGE CFD. The simulation results were then compared to the actual test results. The CFD model shows that it could be an effective tool for predicting the performance of the Oxiperator, though there are many areas for improvement. This research contributes to the development of methane emissions control technologies for lean burn natural gas engines and identifies considerations for improvements on the future Oxiperator design.

TABLE OF CONTENTS

ABSTRACT ii
LIST OF TABLES v
LIST OF FIGURES vi
LIST OF ACRONYMS viii
1. INTRODUCTION 1
1.1 Background 1
1.1.1 Sources of Methane Emissions 1
1.1.2 Government Sanctions on Methane 3
1.1.3 Methane Slip 4
1.2 Literature Review 7
1.2.1 In Cylinder Methane Emission Reduction Technologies 7
1.2.2 Catalytic Oxidation 8
1.2.3 Regenerative Thermal Oxidizer 10
1.2.4 Exhaust Gas Recirculation 12
1.3 Thesis Overview 13
2. METHODS AND MATERIALS 15
2.1 Cummins QSK19G 16
2.2 Third Part Hardware 16
2.2.1 Throttle Actuator 17
2.2.2 Air Fuel Ratio Control 17
2.2.3 CPU 18
2.3 Test Cell Conversion 18
2.3.1 Piping 19
2.3.2 Drive Shaft Shield Installation 20
2.3.3 Pressure transmitters 21
2.3.4 Thermocouples 22
2.4 Exhaust Slipstream 23
2.5 Exhaust Emissions Measurements 24
2.5.1 Fourier Transfer Infrared Gas Analyzer: MKS Instruments, Inc Model No. 2030 FTIR 24

2.5.2 5-gas Analyzer: California Analytical Instruments 700 LX Series 25
2.6 Simplified Oxiperator Schematic 27
2.7 Oxiperator Initial Design 29
2.8 Oxiperator Final Design 32
2.9 CONVERGE CFD 33
3. OXIPERATOR EXPERIMENTAL PERFORMANCE EVALUATION 35
3.1 Cummins QSK19G Baseline Testing 35
3.2 Oxiperator Performance Testing 37
3.2.1 Minimum THC Concentration 40
3.2.2 Minimum Recoverable Temperature 41
3.2.3 Temperature Decay 43
3.2.4 Percentage of Engine Fuel Flow 47
3.2.5 Oxiperator Effectiveness 48
4. COMPUTER SIMULATION OF SUBSCALE OXIPERATOR 49
4.1 Simplifying the Model 49
4.2 Heat up Simulation 50
4.3 Cool off Simulation 51
4.4 Final Oxiperator CONVERGE Simulation 53
5. SUMMARY AND CONCLUSION 56
REFERENCES 59
APPENDIX A 63
APPENDIX B 66
APPENDIX C 69
APPENDIX D 71

LIST OF TABLES

Table 1: 5-gas Analyzer Measurement Methodologies 26

Table 2: Inconel composition and properties [41] 30

Table 3: Engine operating conditions and unaltered engine emissions data 39

Table 4: Light off temperatures of key hydrocarbons and regulated species. Note: the reduction efficiency of Propane only reached as low as 53.8% at the time of shut off with the temperature being 646 (°C). 46

Table 5: Summary of Oxiperator recuperator effectiveness during testing 48

Table 6: Light off temperature of methane inside the reactor portion of the Oxiperator at different lambda values from the CONVERGE CFD simulation. 51

Table 7: Exhaust Concentration for Final Oxiperator Simulation 54

LIST OF FIGURES

Figure 1: EPA reported estimates of sources of methane using data from 1990-2021 [1,2]. 2

Figure 2: Diagram of blow-by in an internal combustion engine [20]. 5

Figure 3: Diagram of valve overlap occurring between exhaust and intake stroke [21]. 6

Figure 4: Percentage of methane conversion for Pd, Pt, Pt:Pd, Rh, and Ni:Mg catalysts with respect to gas temperature [28,32–36], incudes exhaust temperature ranges for 2-stroke and 4-stroke lean-burn natural gas engines [29–31]. data used to generate this figure is summarized in Table A-1. 10

Figure 5: Regenerative Thermal Oxidizers schematics, (a) RTO in which valves 1 and 4 open for flow to go left to right valves 2 and 3 for flow to go right to left [42]. (b) RTO in which flow switches from clockwise to counterclockwise [39]. 11

Figure 6: Overall Schematic of Test Layout 15

Figure 7: Altronic Controls Panel 16

Figure 8: ActuCOM R8 speed governor mounted on the top of the engine using new steel bracket. 17

Figure 9: Cummins QSK19G Test Cell 19

Figure 10: Inlet Air Filter 20

Figure 11: Drive Shaft Shield 21

Figure 12: Rosemount Pressure Transducers 22

Figure 13: Oxiperator Test Layout Diagram 23

Figure 14: MKS Instruments, Inc Model No. 2030 FTIR Gas Analyzer 25

Figure 15: California Analytical Instruments 700 LX Series Analyzers 27

Figure 16: Simplified diagram of the Oxiperator 28

Figure 17: Oxiperator Initial Design Test Skid at University of California – Davis 29

Figure 18: Oxiperator Flow Diagram 31

Figure 19: Bulging of the Initial Oxiperator 32

Figure 20: Final Oxiperator 33

Figure 21: Exhaust composition and temperature of the Cummins QSK19G at different lambda set points. All concentrations have been normalized at 15% O2 using equation 1 [48] 36

Figure 22: LabVIEW Layout of Final Oxiperator Design 38

Figure 23: Oxiperator Maximum temperature trends at different concentrations of THC 41

Figure 24: Temperature of Oxiperator after additional natural gas was added during cool off, the legend includes the THC inlet concentration for each temperature 42

Figure 25: Reduction efficiency of different common hydrocarbons in the exhaust 44

Figure 26: Reduction of VOC and Formaldehyde as well as the CO production rate of the Oxiperator 45

Figure 27: Natural gas required in terms of percentage of engine fuel flow to reach key THC concentrations in the exhaust 47

Figure 28: CONVERGE CFD model of Initial Oxiperator 49

Figure 29: CONVERGE simulation heat up results 50

Figure 30: CONVERGE simulation Cool off results 52

Figure 31: CONVERGE CFD model of the Final Oxiperator 53

Figure 32: Change of Methane Concentration and wall temperature during the Final Oxiperator Simulation, the incoming gas was set at 800 K with a THC concentration of 4400 ppm 55

LIST OF ACRONYMS

C_2H_2 ..... Acetylene
C_2H_4 ..... Ethylene
C_2H_6 ..... Ethane
C_3H_8 ..... Propane
CFD ..... Computational Fluid Dynamics
CH_2O ..... Formaldehyde
CH_3OH ..... Methyl Alcohol
CH_4 ..... Methane
CO ..... Carbon Monoxide
CO_2 ..... Carbon Dioxide
EGR ..... Exhaust Gas Recirculation
EIA ..... Energy Information Administration
EPA ..... Environmental Protection Agency
FID ..... Flame Ionization Detector
FTIR ..... Fourier Transform Infared
GHG ..... Green House Gas
GHGRP ..... Greenhouse Gas Reportin Program
H_2O ..... Water
H_2S ..... Hydrogen Sulfide
hp ..... Horsepower
IR ..... Infared
kg/kmol ..... Kilograms per Kilomole
kJ/mol ..... Kilojule per Mole
kW ..... Kilowatt
kWh ..... kilowatt-hour
kWm ..... Kilowatt Mechanical
Mg ..... Magnesium
MMBtu ..... One Million British Thermal Units

N_2 ..... Nitrogen

N_2O ..... Nitrous Oxide

NH_3 ..... Ammonia

Ni ..... Nickel

NO ..... Nitrogen Oxide

NO_2 ..... Nitrogen Dioxide

NO_x ..... Nitric Oxide and Nitrogen Dioxide

NPT ..... National Pipe Tapered

NSPS ..... New Source Performance Standard

O_2 ..... Oxygen

Pd ..... Palladium

ppm ..... Part per Million

ppmvd ..... parts per million by volume, dry

Pt ..... Platinum

RCO ..... Regenerative Catalytic Oxidizers

Rh ..... Rhodium

rpm ..... Rotations per Minute

RTO ..... Regenerative Thermal Oxidizer

SCFM ..... Standard Cubic Feet per Minute

SO_2 ..... Sulfur Dioxide

THC ..... Total Hydro Carbons

VAM ..... Ventilation Air Methane

VDC ..... Voltage Direct Current

VOC ..... Volatile Organic Compounds

W/m K ..... Watt per Meter Kelvin

1. INTRODUCTION

1.1 Background

Methane (CH_4) is the second most abundant human-generated greenhouse gas (GHG) after carbon dioxide (CO_2). In 2021, methane accounted for approximately 12% of human-induced GHG emissions, with the total emissions reaching 25.98 million metric tons [1,2]. Although methane has a much shorter atmospheric lifespan than CO_2, methane is 25 times more effective at trapping heat in the atmosphere [3,4]. Over the past two centuries, atmospheric concentrations have doubled, and methane now makes up 20% of total global emissions (both natural and human created) [3].

1.1.1 Sources of Methane Emissions

Figure 1 shows EPA reported data for sources of methane emissions in the United States. Methane emissions are a result of various sources, with natural gas and petroleum sources being the largest contributors [1]. As natural gas is composed of 70-90% methane, its uses play a key role in methane emissions [5]. One of the main uses for natural gas engines is power generation. About 38% of the United States' natural gas consumption in 2022 was for electrical power generation [6].

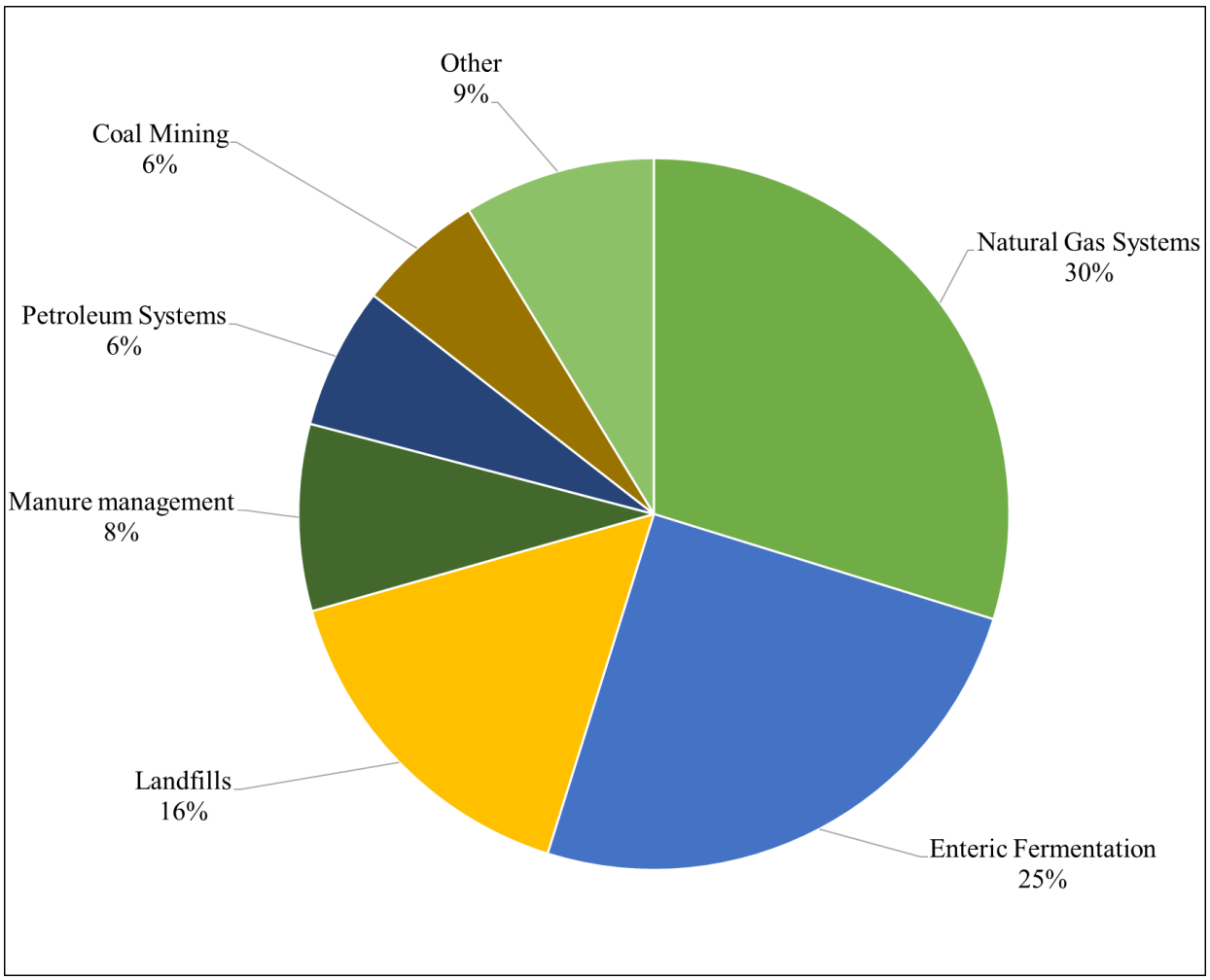

Figure 1: EPA reported estimates of sources of methane using data from 1990-2021 [1,2].

In 2022, according to the Energy Information Administration (EIA), there were roughly 1500 operable natural gas internal combustion engines in the United States being used for power generation [7]. The United States' natural gas consumption for transportation was 5% in 2022. This includes natural gas engines that are used to drive compressors on gas pipelines, as well as natural gas engines that are used in vehicles [6]. The EIA also reports that there are more than 1400 interstate natural gas compression stations that use natural gas engines in the United States [8].

Methane slip is a term that refers to methane that does not combust in a combustion engine. Methane emissions due to methane slip in natural gas systems was 197,000 metric tons in 2020 [2]. Methane slip resulted in 3.0% of all methane emissions from natural gas systems in 2020 [2]. Lean-burn natural gas engines result in higher methane emissions than stoichiometric natural gas engines. Stoichiometric engines, also known as "rich-burn" natural gas engines, are engines that operate at approximately stoichiometric, though slightly rich, air fuel ratios. Stoichiometric engines result in more complete combustion and less unconsumed methane being released via the exhaust than lean-burn natural gas engines [9]. In a study, a 4-stroke stoichiometric engine produced 0.23 lb. of CH_4 per MMBtu while a 4-stroke lean-burn engine produced 1.25 lb. of CH_4 per MMBtu [10]. Stoichiometric engines typically use 3-way catalysts that are effective at reducing methane emissions and are partly responsible for lower methane emissions from this engine class. However, 3-way catalysts are designed for stoichiometric engines and are not effective for lean-burn natural gas engines [9]. Lean-burn natural gas engines are more efficient and are commonly chosen over stoichiometric engines where minimizing fuel consumption is favored. By finding effective methane emission reduction methods for lean-burn natural gas engines, the amount of methane released into the atmosphere can be reduced.

1.1.2 Government Sanctions on Methane

The Greenhouse Gas Reporting Program (GHGRP), which was codified by Title 40 (Protection of Environment) of the code of federal regulations, is used to monitor sources of greenhouse gas emissions around the country. Facilities are required to report their greenhouse gas emissions under the GHGRP [11]. Subpart W of the GHGRP requires petroleum and natural gas facilities that emit the equivalent of 25,000 metric tons of CO_2 of greenhouse gases a year to report

their emissions data to the environmental protection agency (EPA) [12]. Under the Inflation Reduction Act, starting in 2024, facilities that are required to report to the EPA under subpart W will be required to pay $900 per metric ton of CH_4 emitted. This monetary value increased to $1200 in 2025 and to $1500 in 2026 and beyond [13]. For reference, if a facility emits 900 metric tons of CH_4, the equivalent of 25,000 metric tons of CO_2, in 2026, they will be charged $1.5 million dollars. The EPA proposed "Good Neighbor Plan" will require upwind states to decrease their greenhouse gas emissions, including methane, to benefit downwind states [14]. Under subpart JJJJ in the new source performance standard (NSPS) the emissions of stationary natural gas engines are regulated on their emission of volatile organic compounds (VOC). Non-emergency natural gas more powerful that 100 hp are restricted to either 0.7 g/hp-hr or 80 ppmvd (parts per million by volume, dry) at 15% O_2 [15]. VOCs are defined as non-methane, non-ethane hydrocarbons, so they do not include methane [16]. Aldehydes are also excluded from the VOCs. Methane emissions are targeted in impending regulations through the Inflation Reduction Act and Good Neighbor Plan [13,14]. Once these are implemented, the need for technologies to decrease methane emissions becomes more important.

1.1.3 Methane Slip

Methane slip refers to methane that does not combust in the operation of a natural gas engine. Between 1% and 5% of the total methane can "slip" through the system [17]. There are several sources of methane slip in the operation of a natural gas engine, including blow-by, valve overlap, and incomplete combustion.

In a numerical analysis of a lean-burn 4-stroke dual-fuel engine, valve overlap resulted in around 30% of the total methane slip at full load [18]. Incomplete combustion from crevices and

quenching contributed to the other 70%. Blowby was not considered in this analysis. In this study, valve overlap and incomplete combustion from crevices each resulted in the emission of around 10 g of CH_4 per kWh at any load. Methane slip due to quenching caused 10 g of CH_4 per kWh at full load, and 55 g of CH_4 per kWh at 25% load.

Blow-by, shown in Figure 2, occurs when methane leaks between the piston ring and the cylinder wall into the crankcase. Unlike the other sources of methane slip, blow-by does not result in unburned methane in the exhaust and therefore is not able to be treated by any exhaust treatment. Blow-by can result in up to 25% of the methane emissions from a natural gas engine [19].

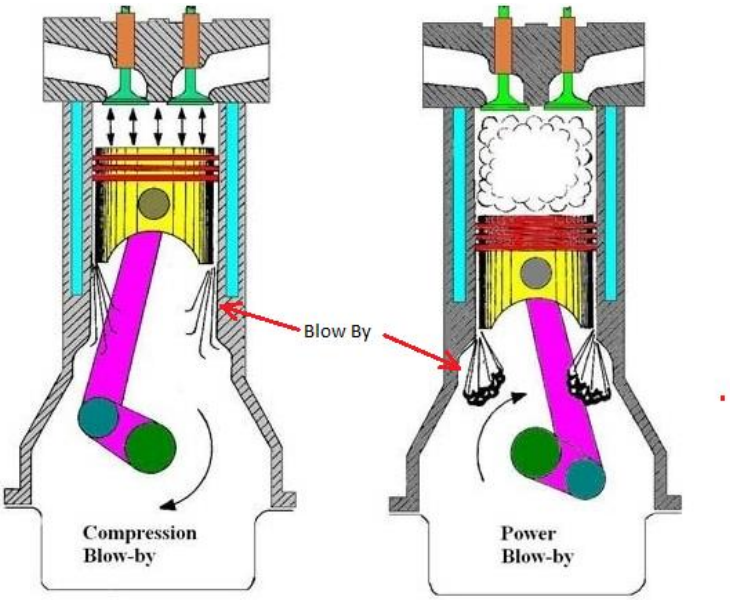

Figure 2: Diagram of blow-by in an internal combustion engine [20].

Valve overlap (see Figure 3) occurs when both the inlet and outlet valves are open, and methane bypasses the combustion process and passes into the exhaust. Valve overlap occurs at the end of the exhaust stroke and the beginning of the intake stroke. During the exhaust stroke (up stroke), the exhaust is being forced out of the cylinder through the exhaust valve. The inlet valve

opens as the piston approaches top dead center. There is a moment when both the inlet and outlet valves are open at the same time. During this time, the high pressure of the incoming gas flows to the low pressure of the exhaust causing methane to go directly from the inlet manifold to the exhaust manifold, resulting in unburned fuel in the exhaust [17].

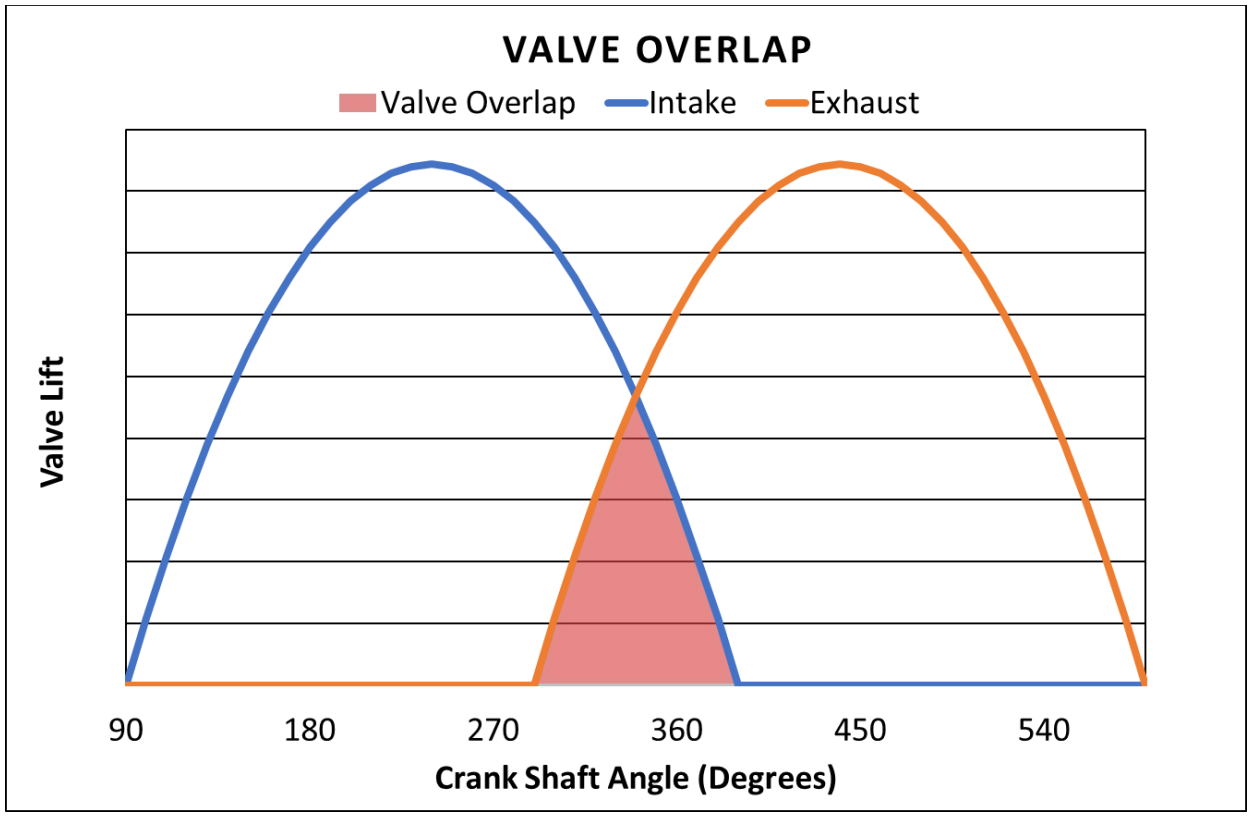

Figure 3: Diagram of valve overlap occurring between exhaust and intake stroke [21].

Incomplete combustion can be a result of trapped methane in crevices, quenching near walls and quenching in lean mixture zones. Crevices (high surface/volume ratio areas) can restrict flame propagation into these areas allowing methane to go unburned [9]. The amount of unburned hydrocarbons increases exponentially with crevice volume [20]. Quenching effects can also result in incomplete combustion. A quenching effect can occur near the walls of the cylinder. Heat is lost

from the gas to the cylinder wall, decreasing the temperature of the gas, not allowing combustion to occur. Quenching can also occur when there are areas of high λ. Lambda (λ) is the ratio of the actual air fuel ratio to the stoichiometric air fuel ratio. In areas of high λ there is not enough fuel for combustion to occur.

1.2 Literature Review

The majority of this section, as well as the previous section, comes from a literature review titled "Methane Emissions Reduction Technologies for Natural Gas Engines: A Review" that was written as a part of this research. This review was submitted to and published in the Energies journal in October 2023 [21].

1.2.1 In Cylinder Methane Emission Reduction Technologies

The way to decrease blow-by is to decrease the clearance between the piston ring and the cylinder wall, improving the seal and decreasing the amount of gas that can slip into the crankcase. The tradeoff of this is the improved seal increases the resistance of the piston decreasing the efficiency of the engine. The methane that leaks into the crankcase creates pressure in the crankcase that needs to be vented. The vented methane from the crankcase can be recycled back into the engine, but it needs to be filtered. Any oil in the methane that was picked up in the crankcase needs to be removed or damage to the engine may occur [17].

Methane slip from valve overlap can be reduced by optimizing the timing for the valves. Valve overlap is necessary because it maximizes the fuel air mixture mass in the cylinder, maximizing performance [17]. Due to the benefits, valve overlap is tolerable considering it only results in minimal methane slip.

To reduce trapped methane in crevices, the piston casing can be redesigned to decrease the size and number of crevices. Redesign of the piston head and/or piston casing can also reduce quenching. Redesign can improve mixing within the combustion chamber and reduce areas of high λ.

One way to decrease quenching effects in the combustion chamber is to operate the engine closer to stoichiometric [9]. With more fuel in the combustion chamber, there is a reduced chance of higher λ areas or heat loss to the cylinder walls resulting in quenching. When operating with a richer mixture, more nitrogen oxides (NOx) are created due to the higher combustion temperatures [22]. Having improved air-fuel mixing, which creates a homogenous mixture, can reduce high λ areas and decrease quenching in a lean-burn natural gas engine [9]. For a lean-burn natural gas engine, running rich is not an option. Controlled auto-ignition is a method which results in stable combustion and less unburned fuel [23]. One way this can be achieved is by design changes to the precombustion chamber nozzle [24]. High pressure fuel injection and precombustion chamber ignition can reduce the frequency of partial combustion and misfires, leading to less methane emissions [25].

1.2.2 Catalytic Oxidation

Catalytic oxidation is a process in which the exhaust flows over a catalyst, usually utilizing a precious metal like palladium or platinum in the case of a methane oxidizer. The catalyst speeds up the process of methane reacting with oxygen and becoming CO_2 and H_2O. Catalytic oxidizers can be susceptible to poisoning and aging. Catalytic poisoning is a deactivation of the catalyst. This can be a result of the poison chemically altering the catalyst, causing it to be less effective or it could simply physically block the catalyst from reacting with the methane [26]. Hydrogen

Sulfide (H_2S) can be present in natural gas at concentrations as high as 5% [5]. The presence of hydrogen sulfide in the combustion process results in sulfur dioxide (SO_2) being produced and present in the exhaust of natural gas engines [27]. Concentration as low as 20 ppm of SO_2 can be detrimental to a catalyst's performance [28]. The source of sulfur in a natural gas engine's exhaust can be from the natural gas itself, but it can also be from the lubrication oil of the engine [27].

Figure 4 plots methane conversion vs. temperature for catalyst studies reported in the literature. The yellow symbol represents palladium catalyst, purple represents platinum catalyst, red represents platinum-palladium alloy catalyst, orange represents rhodium catalyst, and blue represents nickel-magnesium alloy. Each catalyst has an ellipsoid to group the catalyst's performance range. The shaded sections represent exhaust temperature ranges for 4-stroke and 2-stroke lean-burn natural gas engines. The exhaust temperature range for 2-stroke lean-burn natural gas engines is 280-380°C. For 4-stroke lean-burn natural gas engines, it is 395-520°C [29–31]. Light gray represents 2-stroke and dark gray represents 4-stroke.

Platinum and nickel-magnesium catalysts are unable to achieve 100% methane conversion at low enough temperature for either type of lean-burn natural gas engines. Palladium and rhodium catalysts could achieve 100% conversion at temperature within the 4-stroke temperature range, but not the 2-stroke temperature range. Platinum-palladium catalyst is the only catalyst that could achieve 100% conversion within the temperature range of the 2-stroke natural gas engine. The overwhelming majority of studies focusing on oxidation of methane, including the ones summarized in Figure 4, are small scale tests either using bottled gas or just a portion of the exhaust off a natural gas engine.

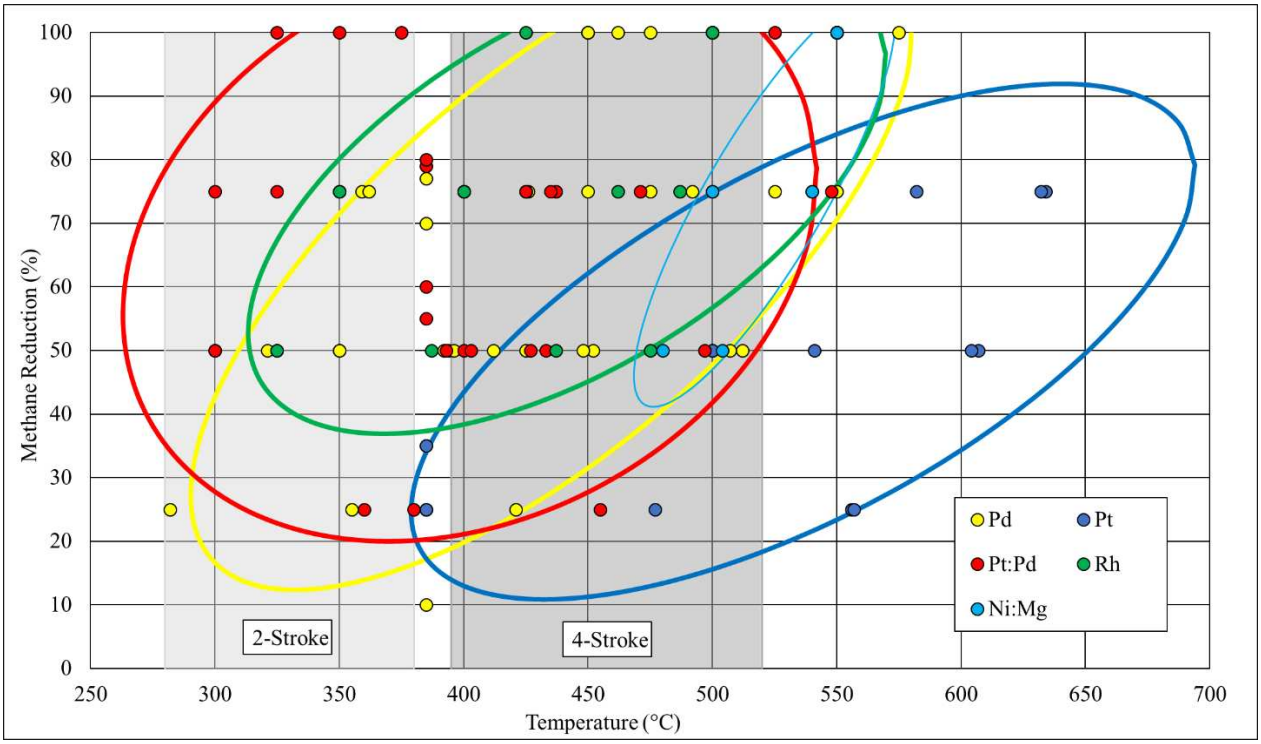

Figure 4: Percentage of methane conversion for Pd, Pt, Pt:Pd, Rh, and Ni:Mg catalysts with respect to gas temperature [28,32–36], incudes exhaust temperature ranges for 2-stroke and 4-stroke lean-burn natural gas engines [29–31]. data used to generate this figure is summarized in Table A-1.

1.2.3 Regenerative Thermal Oxidizer

One method to oxidize methane that does not require a catalyst is a regenerative thermal oxidizer (RTO). Many RTOs consist of two porous heat beds connected by an oxidation chamber [37]. Figure 5 shows the schematics of two different RTOs. The heat beds are usually made from ceramic, though there are instances where they are made of gravel supported by a steel structure [37,38]. In an RTO, the exhaust gas containing methane flows through the first heat bed which acts as a preheater. Once the exhaust reaches temperature, the methane oxidizes and releases heat.

Methane oxidation releases 802.7 kJ/mol, see eqn. 1 [39]. The gas then leaves the oxidation chamber and transfers heat to the second heat bed, which acts as a heat sink. To maintain this process flow through, the RTO is periodically reversed and the second bed becomes the preheater, and the first bed becomes the heat sink. Once the system is operational, it can sustain itself, as the energy release from the oxidation process provides heat to sustain the process. When an RTO is initially started, energy is required to heat the gas to instigate oxidation. Electrical heaters are used in the oxidation chamber to achieve this. These heaters can be in the range of 22-40 kW depending on the size of the RTO [37–40].

$$CH_4 + 2O_2 \rightarrow CO_2 + 2H_2O \qquad \Delta H_{298} = -802.7\frac{kj}{mol} \qquad (1)$$

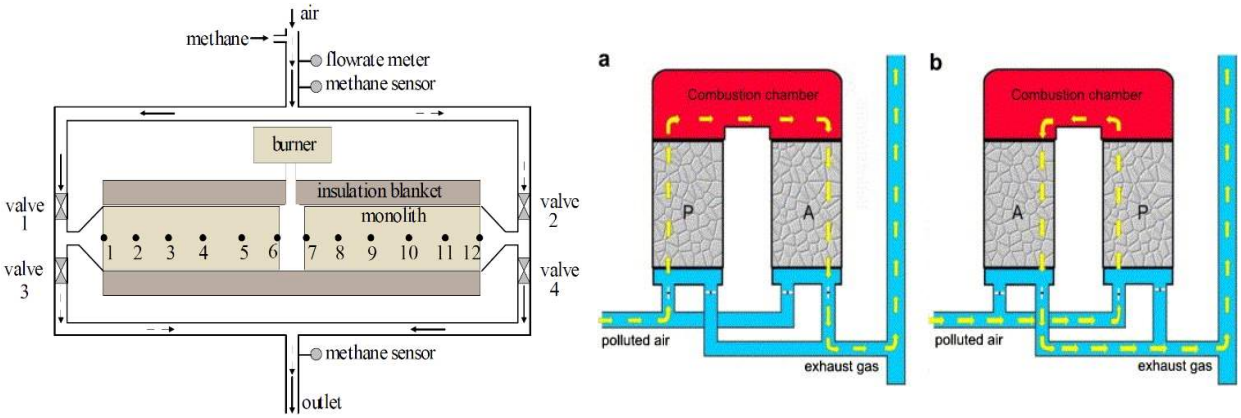

a) b)

Figure 5: Regenerative Thermal Oxidizers schematics, (a) RTO in which valves 1 and 4 open for flow to go left to right valves 2 and 3 for flow to go right to left [42]. (b) RTO in which flow switches from clockwise to counterclockwise [39].

The primary use of RTOs has been to oxidize methane gas from ventilation air methane (VAM) found in coal mines [41]. Due to their size and complexity, there have not been many applications for using RTOs on natural gas engines. The benefit of using an RTO to oxidize

methane in the exhaust of a lean-burn natural gas engine is that no matter what the temperature of the exhaust gas is, it can be heated to induce oxidation. The exhaust temperature range for 2-stroke and 4-stroke lean-burn natural gas engines are 280-380 °C and 395-520 °C respectively [29–31]. There may not be a need for heat to be added for a 4-stroke engine operating within the higher range of exhaust temperatures. For the lower end of the exhaust temperature range for 4-stroke engine, and for the entire 2-stroke exhaust temperature range, heat will need to be added to the combustion chamber to induce oxidation.

Regenerative Catalytic Oxidizers (RCO) have a similar layout to an RTO, but have a catalyst in the heat bed. This can decrease the operating temperature required for complete oxidation, with many RCOs requiring 320-430 °C, while RTOs require ranges closer to 760-820 °C. A study using a RCO on a natural gas/diesel dual-fuel engine saw more than 90% reduction in hydrocarbon emissions [42]. This RCO operated at temperatures between 300-700 °C.

1.2.4 Exhaust Gas Recirculation

Exhaust gas recirculation (EGR) is a process in which a portion of the exhaust gas is recirculated back into the engine. The methane in the exhaust that is recirculated will be used in the combustion process [9]. Up to 25% of the exhaust is used in an EGR system while up to 75% of the exhaust goes untreated for methane slip unless another method of methane reduction is used. With EGR rates above 25%, the cylinder pressure and brake efficiency drop off significantly [43]. An intercooler is required to cool the exhaust. The intercooler can result in water droplets forming which can increase wear on the turbocharger [9]. An EGR system can result in a 20% reduction of methane emissions [44]. A study performing EGR sweeps on a natural gas engine saw a 45% reduction of methane emissions using an EGR rate of 14.7% [30]. EGR would need to be paired

with another methane emission reduction methods such as catalytic oxidizer or an RTO to achieve 100% methane reduction. Other benefits to an EGR system are improved combustion stability and decrease in NO_x emissions [9,44].

1.3 Thesis Overview

The primary objective of this thesis is to answer the following question: can a thermal oxidizer on a lean-burn industrial natural gas engine be self-sustaining with only the energy input from exhaust hydrocarbon and CO emissions? If not, what are the required parameters for a self-sustaining operation? To answer this question, a Cummins QSK19G lean burn natural gas engine was commissioned at the Energy Institute at Colorado State University for this project. The thermal oxidizer previously mentioned is called an Oxiperator, a device created by Prabhu Energy Labs, a company based out of Mission Viejo, California.

Baseline testing was performed on the Cummins QSK19G to determine what optimal operating point would be best for Oxiperator testing. The Oxiperator was then brought to Colorado State and was tested using the exhaust of the Cummins QSK19G. A slip stream, which is a branching route for the exhaust, was used in testing the Oxiperator. Only a portion of the engine's exhaust flow was used, as the Oxiperator was designed for 50 SCFM, while the flow from the engine is significantly higher. Gas composition sampling took place at the inlet and outlet of the Oxiperator and was measured using both an FTIR spectrometer and a set of EPA regulations compliant gas analyzers.

Additionally, computer simulations using CONVERGE CFD were performed to evaluate the effectiveness of using CONVERGE CFD as a prediction model for thermal oxidizers.

Computer models of the Oxiperator were created. Data from the exhaust temperature and emissions from the engine, as well as the Oxiperator's internal temperature, were used in model setup. The performance of the Oxiperator was compared to the CONVERGE CFD model results.

2. METHODS AND MATERIALS

The Cummins QSK19G is a 19-liter natural gas lean burn engine that will be used to produce exhaust to flow through the Oxiperator. A portion of the exhaust will tee off the exhaust stack using a back pressure valve which will flow into the Oxiperator. The slip stream will be used to control the flow through the Oxiperator. Figure 6 shows a simplified schematic of the test layout.

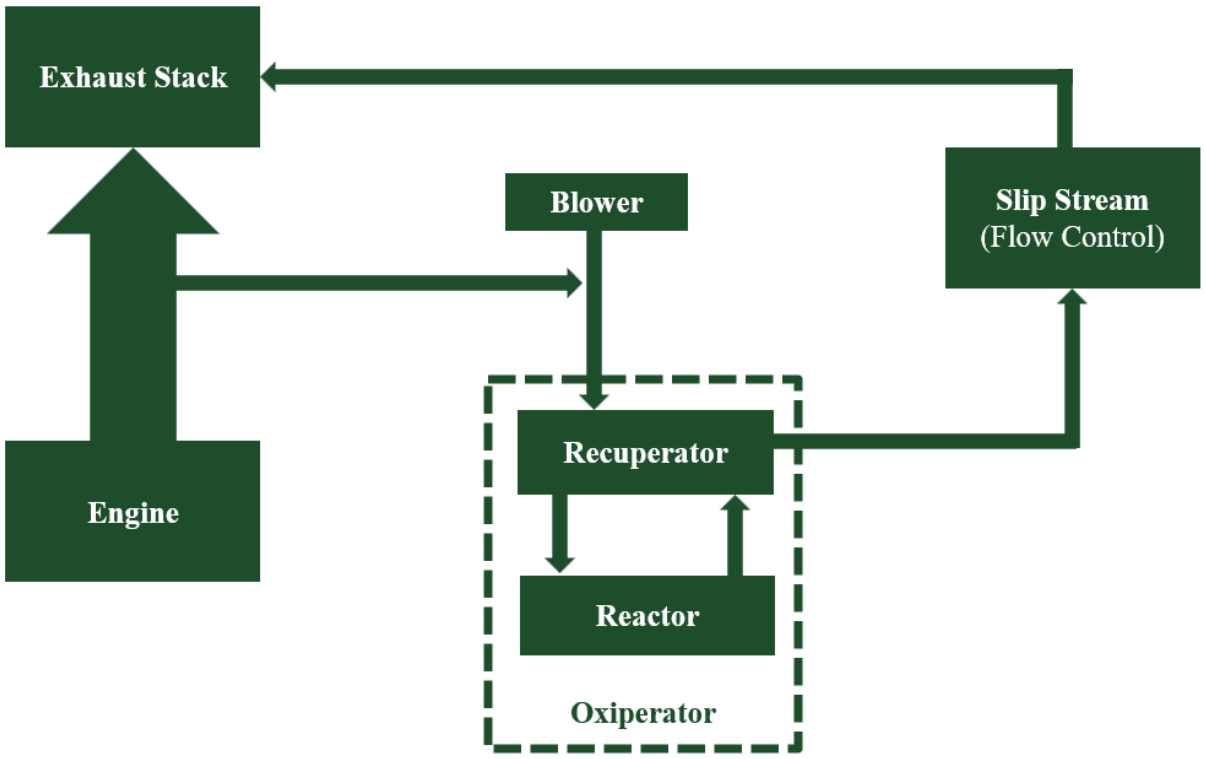

Figure 6: Overall Schematic of Test Layout

2.1 Cummins QSK19G

The Cummins QSK19G is a 19-liter turbocharged natural gas lean burn engine. It has a rated power of 471 horsepower (351 kWm) at a speed of 1800 rpm. It has 6-cylinders in an inline configuration with a compression ratio of 11.0 to 1.0.

2.2 Third Part Hardware

To improve control of the Cummins QSKG19 engine, many of the stock Cummins electronic components were replaced with new controls produced by Altronic LLC. This includes the throttle actuator (ActuCOM R8), Air fuel ratio controller (AFR 500), and CPU unit (CPU 95). These components were donated by Altronic to the project. An additional control panel was installed on the test skid to house the AFR 500 and CPU 95.

Figure 7: Altronic Controls Panel

2.2.1 Throttle Actuator

The stock throttle control was replaced by an ActuCOM R8 integrated gas engine speed governor and smart digital actuator. The ActuCOM R8 is controlled using a serial data link and is powered by a 24 VDC power supply. The ActuCOM R8 requires a magnetic pickup to be installed along the gear teeth of the drive shaft. The ActuCOM R8 did not fit where the original actuator was located. The throttle valve was rotated 90 degrees to point the valve shaft upwards so that the new actuator could be directly above the throttle valve. A steel bracket was designed to hold the actuator in place using the mounting holes for the original actuator.

Figure 8: ActuCOM R8 speed governor mounted on the top of the engine using new steel bracket.

2.2.2 Air Fuel Ratio Control

An AFR-500 advanced air-fuel ratio control system was installed. The installation of the AFR-500 included a new lambda sensor and thermocouple installed on the exhaust stack. The AFR-500 monitors the lambda value in the exhaust and controls the fuel valve to adjust the air fuel ratio to the proper set point.

2.2.3 CPU

An Altronic CPU-95 advanced digital ignition system for industrial engines was installed, along with a digital panel that allows adjustments to be made at the cell. The CPU-95 requires a magnetic pick up along the gear teeth of the drive shaft in addition to the one required by the ActuCOM R8. The CPU-95 reset pin was installed onto the drive shaft to monitor by a magnetic pickup. A magnet was installed onto the camshaft and was monitored by hall-effect cycle sensor. The reset pin and the cycle sensors work in tandem to determine the ignition timing for the CPU-95. New spark plug leads and ignition coils were installed onto the engine with the CPU-95 controlling the ignition timing. A display module was installed with the CPU-95 Ignition module, connected by an RS485 serial data link. The display module allows for the engine's ignition timing to be adjusted right at the test cell.

2.3 Test Cell Conversion

The 19-liter Cummins was previously installed in the same location in the engine lab, but due to the installation of a solar turbine in the engine lab, the entire test skid had been rotated 90 degrees. When re-installing the engine, several adjustments to the test cell were needed.

Figure 9: Cummins QSK19G Test Cell

2.3.1 Piping

All new piping was installed for both the engine and the dyno. The piping required for the engine included intercooler coolant, jacket coolant, fuel, and air. The dyno required a single coolant line. All the coolant and fuel lines are made from schedule 40 black steel. The intercooler coolant lines are 1” NPT threaded pipe, the fuel and dino coolant lines are 2” NPT threaded pipe, and the jacket coolant lines are 3” grooved pipe connected with Gruvlok connections. The original plan for the inlet air was to pipe the air up from the turbo charge in the basement to have the ability to simulate running the engine at sea level. The task of running the air up from the basement was

deemed to be too time-consuming, so it was decided that air would be pulled from the room with a small cylindrical air filter attached instead of a large box filter that would have been used. A model of the piping layout can be found in Appendix B.

Figure 10: Inlet Air Filter

2.3.2 Drive Shaft Shield Installation

The drive shaft connects the engine and the dyno and spins at up 1800 rpm when the engine is running. The drive shaft is a major safety hazard and needs to be properly shielded. The original shield was installed around the drive shaft and consists of two halves that surround it. The new test cell configuration is different from the original. To navigate this difference, a horizontal support was made from a piece of steel c-channel to support the drive shaft shield's feet closest to the engine, see Figure 11.

Figure 11: Drive Shaft Shield

2.3.3 Pressure transmitters

A line of seven Rosemount pressure transmitters were mounted in the center of the test skid to monitor the pressure at various points in our system, see Figure 12. For our testing, we only required two of the Rosemounts to be piped into the system. In addition to the Rosemount pressure transmitters, another Omega brand pressure transmitter was set up specifically for monitoring engine oil pressure.

Figure 12: Rosemount Pressure Transducers

2.3.4 Thermocouples

To monitor key temperatures across the test cell, many K-type omega thermocouples were installed. Locations where thermocouples were placed include intake air, intake manifold, exhaust manifold, and exhaust stack. Thermocouple lead wires were run to the original control box and are monitored through Labview.

2.4 Exhaust Slipstream

The Oxiperator was designed for a flow of 50 SCFM, which is significantly lower than the exhaust flow of the QSK19G engine. To split the exhaust flow, only 50 SCFM is going to the Oxiperator, when a device called a slipstream is used.

A manual back pressure valve was placed on the engine's exhaust stack, along with two tee pipes on either side of the back pressure valve. The Oxiperator and slipstream were placed in series. The Oxiperator inlet is connected to the first tee pipe, the Oxiperator outlet is connected to the slipstream inlet, and the slipstream outlet is connected to the second tee pipe. This creates an "auxiliary" route for the exhaust to flow through.

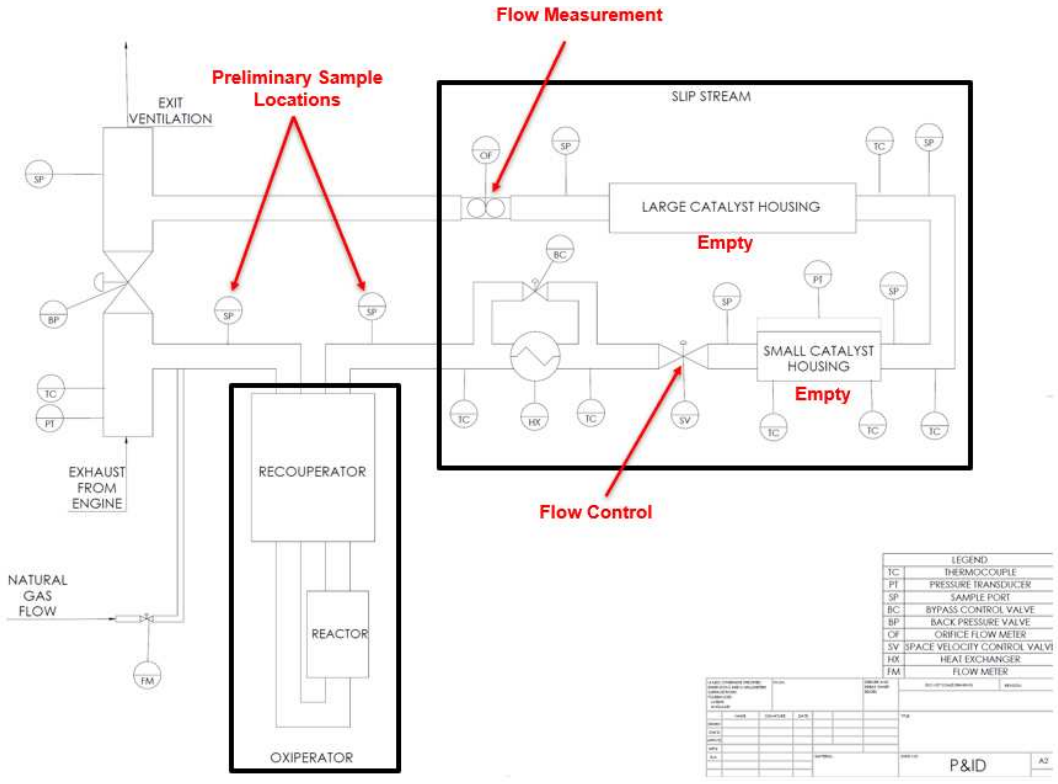

Figure 13: Oxiperator Test Layout Diagram

The back pressure valve is partially closed creating a pressure differential across the valve. This pressure differential drives a portion of the exhaust flow through the Oxiperator and the slipstream. The slipstream uses a feedback loop with an orifice flow meter to monitor the flow going through the device. and an electronic butterfly valve to monitor and control the flow through the slipstream to the setpoint 50 SCFM.

2.5 Exhaust Emissions Measurements

During both the baseline test and Oxiperator test, the emission data was measured using the same means. Gas was extracted from the exhaust using a stainless-steel averaging probe that is used to obtain a sample from the entire cross section of the pipe. The sample is transported to the sampling instrumentation through a heated sample line that is kept at above 100 °C to prevent water condensation.

2.5.1 Fourier Transfer Infrared Gas Analyzer: MKS Instruments, Inc Model No. 2030 FTIR

The Fourier Transfer Infrared (FTIR) Gas Analyzer, see Figure 14, is the main gas analyzer that is used to measure the species concentration in the exhaust gas. The FTIR spectrometer measures the sample “wet”. This means that the sample is still hot and no water condensation has occurred. The FTIR utilizes IR absorption spectra of various exhaust species to quantify the composition of the exhaust. It quantifies any species below a molecular weight of about 45 kg/kmol. This includes any THC up to C_3 as well as NO, NO_2, N_2O, NH_3, H_2O, CO, CO_2, as well as other chemical compounds.

Figure 14: MKS Instruments, Inc Model No. 2030 FTIR Gas Analyzer

2.5.2 5-gas Analyzer: California Analytical Instruments 700 LX Series

The 5-Gas Analyzer, see Figure 15, is a common set of analyzers used for measuring the primary species in IC engine exhaust. These species include CO, CO_2, THC, NO_x, and O_2. Each species uses different measurement techniques that are developed per EPA protocol and is one of the most accurate qualification methods. Unlike the FTIR analyzer, the 5-gas analyzer measures the sample "dry". The sample is run through a Peltier type chiller to condense out all water before

the sample is measured. Table 1 summarizes information on how each species is measured. One of the primary benefits of the 5-gas analyzer over the FTIR gas analyzer is that it can be tied directly into the LabView program that is used to run the engine. This means that we can get real-time measurements while running the engine. Data from the FTIR analyzer is not able to be analyzed until after the fact.

Table 1: 5-gas Analyzer Measurement Methodologies

	Device	**Measurement Technology**	**Minimum Concentration Range**	**Maximum Concentration Range**	**Linearity**
CO	CAI 700 LX NDIR	IR	0-50 ppm	0-100%	1% of full-scale value
CO_2	CAIL 700 LX NDIR	IR	0-50 ppm	0-100%	1% of full-scale value
THC	CAI 700 LX HFID	FID	0-30 ppm	0-30,000 ppm	1% of full-scale value
NO_x	CAI 700 LX CLD	Chemiluminescence	0-3 ppm	0-3000 ppm	1% of full-scale value
O_2	CAI 700 LX NDIR	Paramagnetic	0-1%	0-100%	1% of full-scale value

Figure 15: California Analytical Instruments 700 LX Series Analyzers

2.6 Simplified Oxiperator Schematic

The Oxiperator is a thermal recuperating oxidizer designed by Prabhu Energy Labs based out of Mission Viejo, California. Figure 16 shows a simple diagram on how the Oxiperator works. Exhaust from the engine enters the recuperator and is preheated. The gas enters the reactor and the methane in the exhaust oxidizes. Methane oxidation is an exothermic reaction, meaning heat is released. That excess heat is then dumped into the recuperator preheating the incoming gas. The exhaust, now with a significantly lower methane concentration, is released via the exhaust stack.

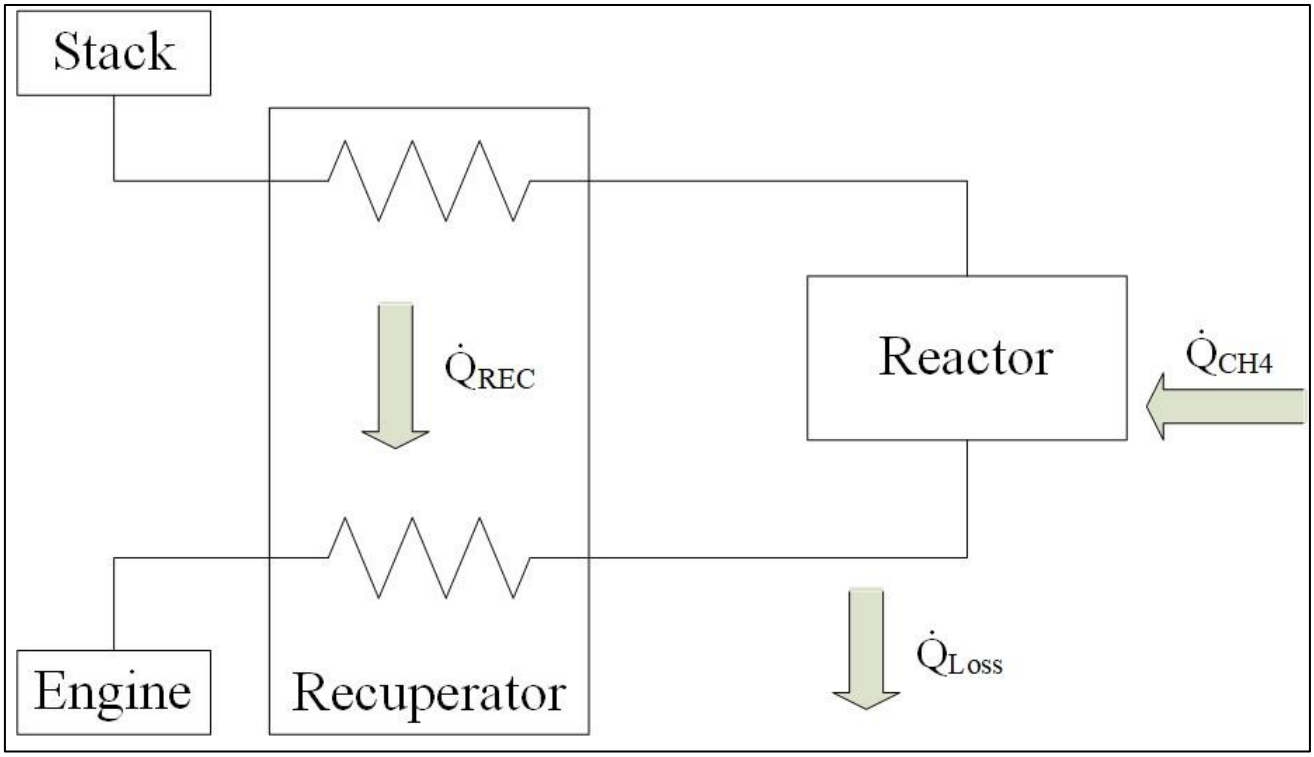

Figure 16: Simplified diagram of the Oxiperator

Methane does not begin to auto-combust until 600 °C [45]. This is significantly higher than the exhaust temperature of both 2-stroke and 4-stroke lean burn natural gas engines. This means additional heat needs to be added to the reactor to initiate the reaction. This comes in the form of a combustor attached to the reactor.

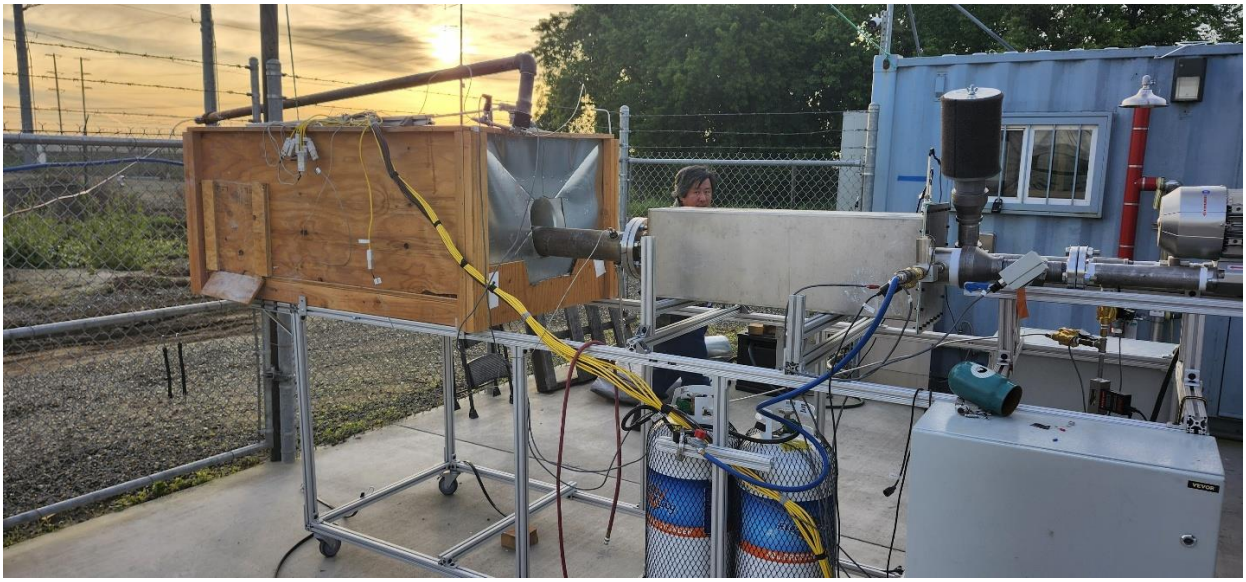

Figure 17: Oxiperator Initial Design Test Skid at University of California – Davis

2.7 Oxiperator Initial Design

The first iteration of the Oxiperator consists of two closely connected halves, a recuperator, and a reactor. The overall assembly is 60 cm long, 20 cm tall, and 20 cm wide. Each half is made up of dozens of short channels that take up the width of the device. The channels alternating flow direction. The reactor channels are 2.3 mm tall and recuperator channel is 1 mm with roughly two recuperator channels per reactor channel. Figures of the initial Oxiperator design and LabVIEW control panels can be found in Appendix B.

The device is made of Inconel 625 and was printed in 3D at Carnegie Mellon University. Inconel 625 is a Nickel base alloy created by Aerospace Specification Metal's base out of Pompano Beach, Florida. Table 2 summarizes the composition of Inconel 625, as well as its relevant physical properties.

Table 2: Inconel composition and properties [41]

Metal	Weight Percentage	Property	Value
Nickel	Min 58%	Specific Heat Capacity	0.41 kJ/kg-°C
Chromium	20-23%	Thermal Conductivity	9.8 W/m-K
Molybdenum	9-10%	Melting Point	1290-1350 °C
Iron	Max 5%	Density	8440 kg/m^3
Niobium	3.15-4.15%	Tensile Strength, Ultimate	880 MPa
Copper	Max 1%	Tensile Strength, Ultimate at 650 °C	760 MPa
Manganese	Max 0.5%	Tensile Strength, Yield	460 MPa
Silicon	Max 0.5%	Tensile Strength, Yield at 650 °C	290 MPa
Aluminum	Max 0.4%		
Titanium	Max 0.4%		
Carbon	Max 0.1%		
Phosphorus	Max 0.015%		
Sulfur	Max 0.015%		

To insulate the device, it is encased in a box filled with FREEFLOW-1000X, which is a pourable thermal powder. FREEFLOW-1000X has very beneficial thermal properties, including a thermal conductivity of 0.064 W/m K and a specific heat capacity of 1.10 kj/kg K at 800 °C. [46]

The flow of gas makes a figure-eight-like path as it travels through the Oxiperator, which can be seen in Figure 18. The gas enters the recuperator on the left side of the device. Each inflow channels is bordered by an outflow channel on both the top and bottom. The gas flows down and across the device, exiting the recuperator on the right side of the device. The gas enters the reactor and flows to the end of the device where there are small holes allowing the gas to flow to either the outflow channels below or above. The gas then flows back towards the front of the device

where it exits the reactor on the left side of the device. It enters the recuperator and flows to the exit on the right side of the device.

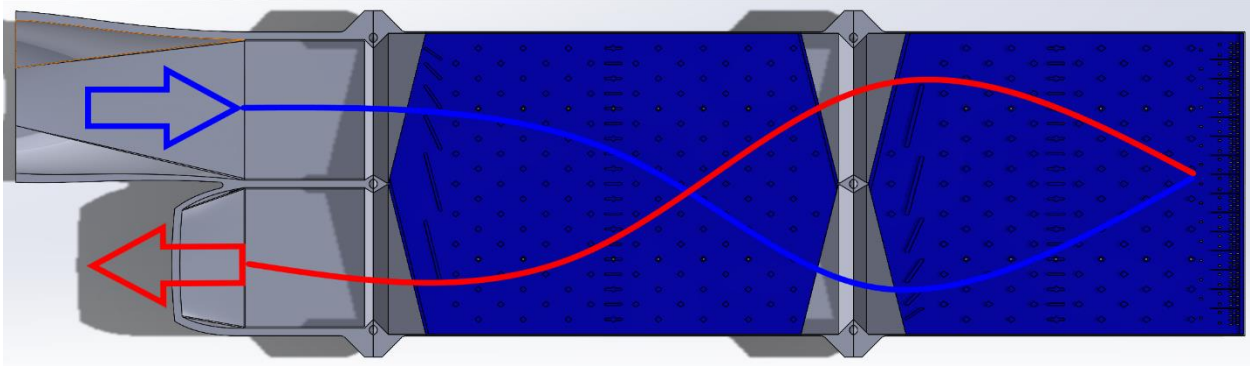

Figure 18: Oxiperator Flow Diagram

In spring of 2024, the Oxiperator was tested at the University of California – Davis by Prabhu Energy Labs. The device was tested using synthetic exhaust, which was just a mix of methane and air. To raise the temperature of the gas to begin combustion, a propane fueled heater was placed at the inlet of the Oxiperator.

After the bench test at the University of California – Davis, there were several problems with the current Oxiperator. The device had been exposed to temperatures too hot for it to handle, and it began to bulge and caused leaks that made the device ineffective. Figure 19 shows images of the bulging that took place.

Figure 19: Bulging of the Initial Oxiperator

2.8 Oxiperator Final Design

Due to the damage incurred by the initial Oxiperator bench testing, it had to be remade. Many alterations were made to the existing design. Prabhu Energy Labs and the University of California – Davis were responsible for all Oxiperator redesigns, as well as all bench testing. The device was simplified significantly: as seen in Figure 20, the recuperator was replaced with a Bosal heat exchanger that was made from Inconel 625, while the reactor was changed to be a U-turn shape of steel tubing. The first half of the U-turn includes a reactor that has an attached natural gas combustor, which is used to initiate the reaction during the warmup process. Figures of the final Oxiperator design and LabVIEW control panels can be found in Appendix B.

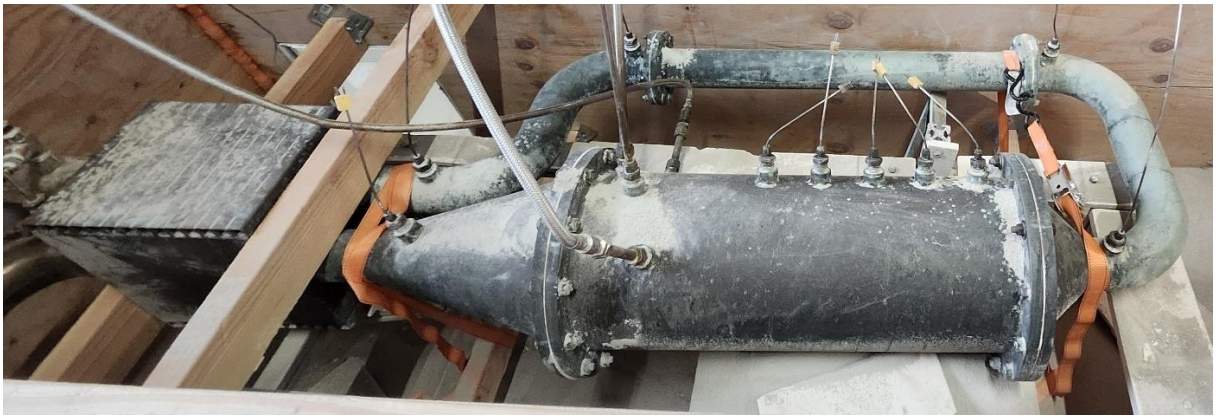

Figure 20: Final Oxiperator

Similar to the initial Oxiperator, the flow through the final Oxiperator made a figure-eight-like pattern through the device. The gas enters the heat exchange and is pre-heated. The gas enters the reactor where the methane and other hydrocarbons are oxidized. The gas then flows back the heat exchanger to pre-heat the incoming gas. The gas then exits the heat exchange and exits the device. A number of k-type thermocouples were installed along the whole flow length of the device to monitor temperatures during testing.

In the fall of 2024, the final Oxiperator was bench tested at the University of California – Davis. The test was considered successful, and the device was then sent to Colorado State University for testing on the Cumins QSK19G.

2.9 CONVERGE CFD

CONVERGE is a computational fluid dynamics (CFD) program that was used to create a 3-D model of the Oxiperator and simulate how its performance. The CONVERGE simulations were compared to the actual performance of the Oxiperator to evaluate the viability of using

CONVERGE to predict the performance of thermal Oxidizers. The simulation uses a chemical kinetic mechanism to predict the behavior of the chemical species in the exhaust.

CONVERGE was developed with an emphasis on engine simulations and used in both engine and non-engine simulations. CONVERGE's grid setup system is automatic, simple, and user-friendly. The computation time required to generate the grid is greatly decreased compared to other CFD programs. CONVERGE is produced by Convergent Sciences which is headquartered in Madison, Wisconsin [47].

3. OXIPERATOR EXPERIMENTAL PERFORMANCE EVALUATION

3.1 Cummins QSK19G Baseline Testing

The goal of the baseline test of the Cummins QSK19G engine is to determine baseline emissions data. This will be used to determine an optimal testing point for the Oxiperator. The most optimal operating point for the Oxiperator is high exhaust methane concentration and high exhaust temperature.

The engine was run at a speed of 1500 rpm and at 100% load. 100% load at 1500 rpm is 402 hp. The load was applied through the dynamometer. The max rated speed for the engine is 1800 rpm, but the engine was unable to run steadily at that speed, so the engine was tested at 1500 rpm. An EQ ratio sweep was performed, with the EQ ratio then swept between the lean and rich limit. At each set point, data was be taken over 3 minutes and averaged. Additional set points were selected and tested based on the results of the EQ ratio and Ignition Timing, with an emphasis on maximizing exhaust temperature and exhaust methane concentration.

The Cummins Engine was tested on August 2, 2024. The engine was run at 1500 rpm at 100% load and with an ignition timing of 10.8° before top dead center. A lambda sweep was performed with a total of six data points ranging from lambda values of 1.08 to 1.40. The data from this test is summarized in Appendix C.

The key parameters, methane concentration and exhaust temperature, are summarized in Figure 21. Methane concentration increases significantly as the lambda values increase, while the exhaust temperature slightly decreases.

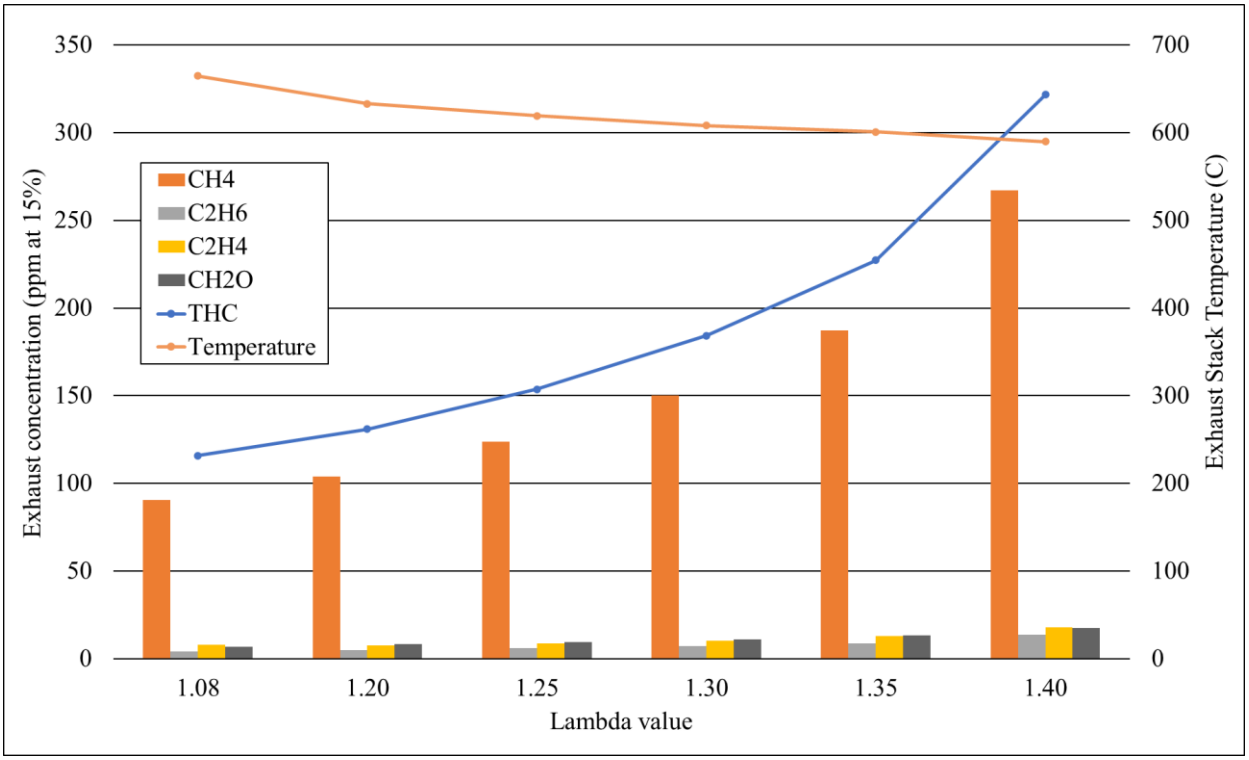

Figure 21: Exhaust composition and temperature of the Cummins QSK19G at different lambda set points. All concentrations have been normalized at 15% O2 using equation 1 [48]

$$Adjusted\ Concentration = Measured\ Concentration * \frac{21 - O_{2_{ref}}}{21 - O_{2_{measured}}} \quad (1)$$

Based on the baseline testing the optimal operating condition of the engine for testing the Oxiperator would be at a lambda value of 1.40. This operating point does have the lowest temperature of the six operating points tested; however, it has the highest concentration of THC in the exhaust, which makes it the optimal choice.

3.2 Oxiperator Performance Testing

The goal of the Oxiperator test was to determine its effectiveness of oxidizing THC (Total Hydrocarbons) for the exhaust of a Cummins QSK19G engine. This test took place over two days, with the first day used as a setup and troubleshooting day that was then used to develop the test plan for the second day. The three questions that were to be answered by the testing were as follows: What is the minimum THC concentration that the Oxiperator needs to maintain Temperature? What is the lowest temperature that the Oxiperator can reach where the reaction can be recovered? How does the THC oxidation efficiency change as the Oxiperator begins to cool off?

Figure 22 shows the final Oxiperator design LabView module which includes the location of the thermocouple locations within the device. For figures throughout this section, when temperature is referred to, the data from thermocouple TC_592 is utilized. This thermocouple was selected because it was the location of highest temperature throughout testing

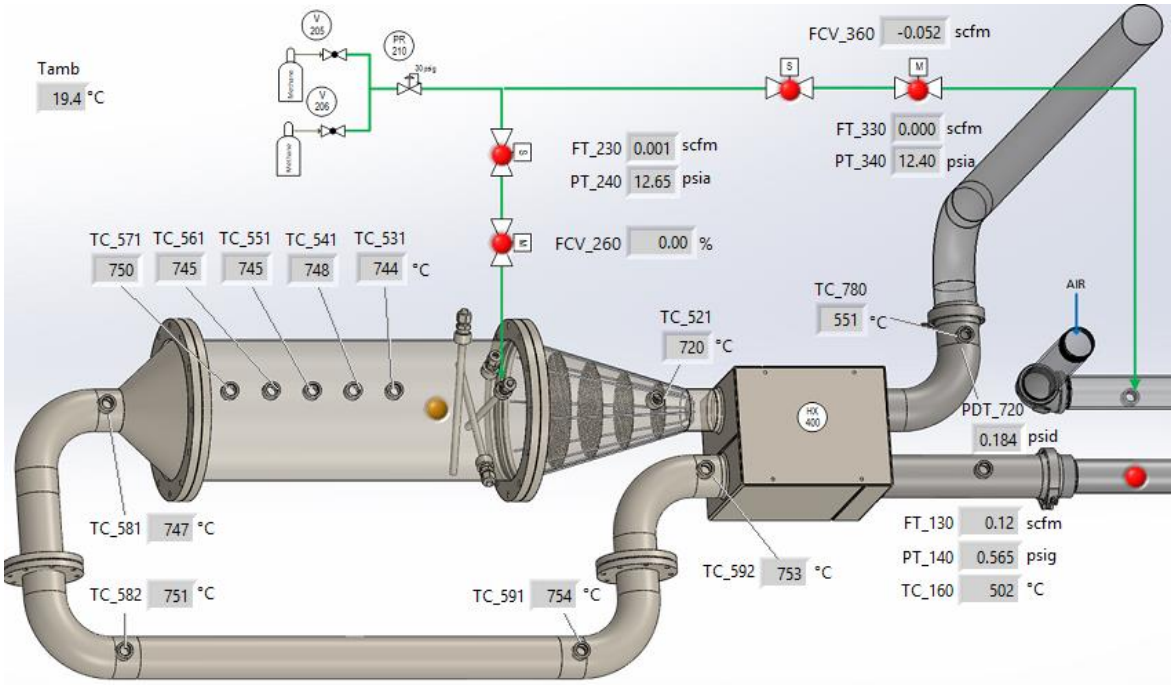

Figure 22: LabVIEW Layout of Final Oxiperator Design

The engine was run at a speed of 1300 rpm and at a load corresponding to 220 hp with a lambda value of 1.10. The load was applied through the dynamometer. From the baseline test that took place in August 2024, the target speed and lambda value were 1500 rpm and 1.40 respectively. Due to control issues, the engine was not able to run stable at that speed and lambda value. The engine had to be run at a slower speed as well as a significantly richer air-fuel ratio. See Table 3 for a summary of the engine operating conditions as well as a summary of emissions data.

Table 3: Engine operating conditions and unaltered engine emissions data

Engine Conditions		Emissions	
Speed	1300 RPM	THC	463 ppm (2.49 g/kW-hr)
Power	220 kW	CO	234 ppm (1.85 g/kW-hr)
Ignition Timing	-10.8 BTDC	NO_X	4652 ppm (60.7 g/kW-hr)
EQ Ratio	0.91	VOC	90.9 ppm (0.802 g/kW-hr)
Exhaust Stack Temperature	600 °C	Methane	372 ppm (1.69 g/kW-hr)
Turbo Inlet Temperature	810 °C	Formaldehyde	25.8 ppm (0.220 g/kW-hr)
Fuel Consumption	89.28 kg/hr	O_2	1.73%

For both days of testing, the Oxiperator was heated independently of the engine. A three-way valve was placed on the inlet of the Oxiperator, with one route coming from the engine's exhaust and the other from an electric blower. Using the blower, 50 SCFM of ambient air flowed through the device where an internal combustor was ignited to begin the heat up process. As the device got to temperature, aspirated natural gas was introduced into the inflow of the Oxiperator. The amount of fuel going to the combustor slowly decreased. Eventually, the fuel to the combustor was completely shut off and the Oxiperator was running solely on the aspirated natural gas. This process of warming up the Oxiperator was similar to what was used for the bench testing of the Oxiperator at the University of California-Davis in Sacramento, California. The bench testing took place before the device arrived at Colorado State University. Once the Oxiperator warmed up with

a max temperature of approximately 925 °C, the three-way valve was switched so that the engine exhaust began to flow through the Oxiperator. The amount of THC in the exhaust was determined to be insufficient to sustain the reaction in the Oxiperator based off the bench testing. To counteract this, additional natural gas was introduced into the exhaust line leading to the Oxiperator via a manual flow meter.

Using the FTIR and 5-gas analyzers, exhaust composition was sampled pre-Oxiperator, as well as post-Oxiperator. The analyzers can only sample one location at a time, so using an automated pneumatic valve, the sampling port measured pre-Oxiperator for 1 minute and then switched to measure post-Oxiperator for 5 minutes, for a total cycle length of 6 minutes.

3.2.1 Minimum THC Concentration

Once the Oxiperator was warmed to temperature and had engine exhaust flowing through it, excess natural gas was added to the exhaust to increase the THC concentration to 8600 ppm. From the initial day of testing, it was determined that the Oxiperator would maintain temperature at this concentration. The temperature of the Oxiperator was closely monitored as the amount of added natural was adjusted. The concentration of THC in the exhaust was slowly decreased until the Oxiperator was no longer able to maintain temperature. The THC reduction efficiency remained 100% throughout this test. Figure 23 shows how the Oxiperator temperature changes at different concentrations.

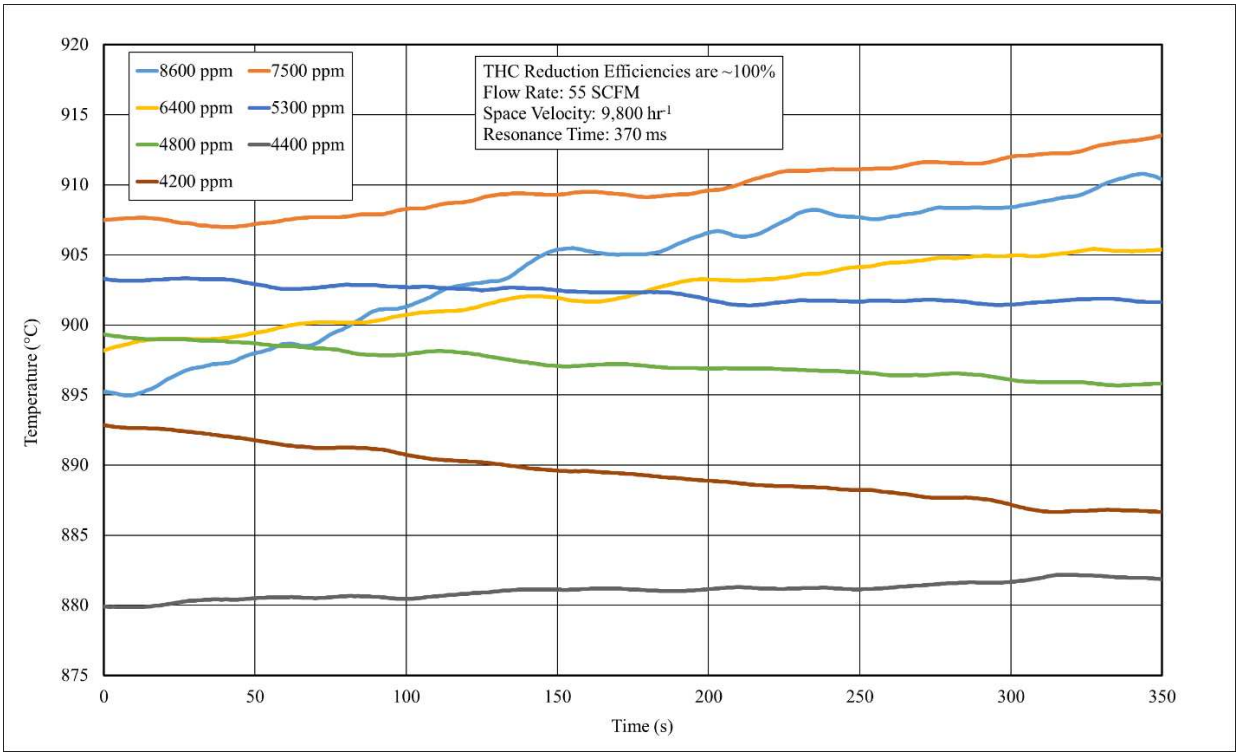

Figure 23: Oxiperator Maximum temperature trends at different concentrations of THC

At THC concentrations of 4400 ppm and above, the temperature of the Oxiperator was able to maintain or increase. At 4200 ppm, the temperature of the Oxiperator slowly decayed and the reaction would most likely stop if left at that concentration indefinitely. A THC of 4400 ppm is the minimum concentration required for the Oxiperator to maintain temperature.

3.2.2 Minimum Recoverable Temperature

To begin the temperature recovery test, the additional natural gas was cut off entirely. Periodically as the Oxiperator cooled off, the supplementary natural gas was turned back on to determine if the temperature of the Oxiperator would begin to recover. This was done at 855 °C,

840 °C, 815°C, and finally at 800 °C. Figure 24 tracks the max Oxiperator temperature after the supplementary natural gas was turned on at each temperature.

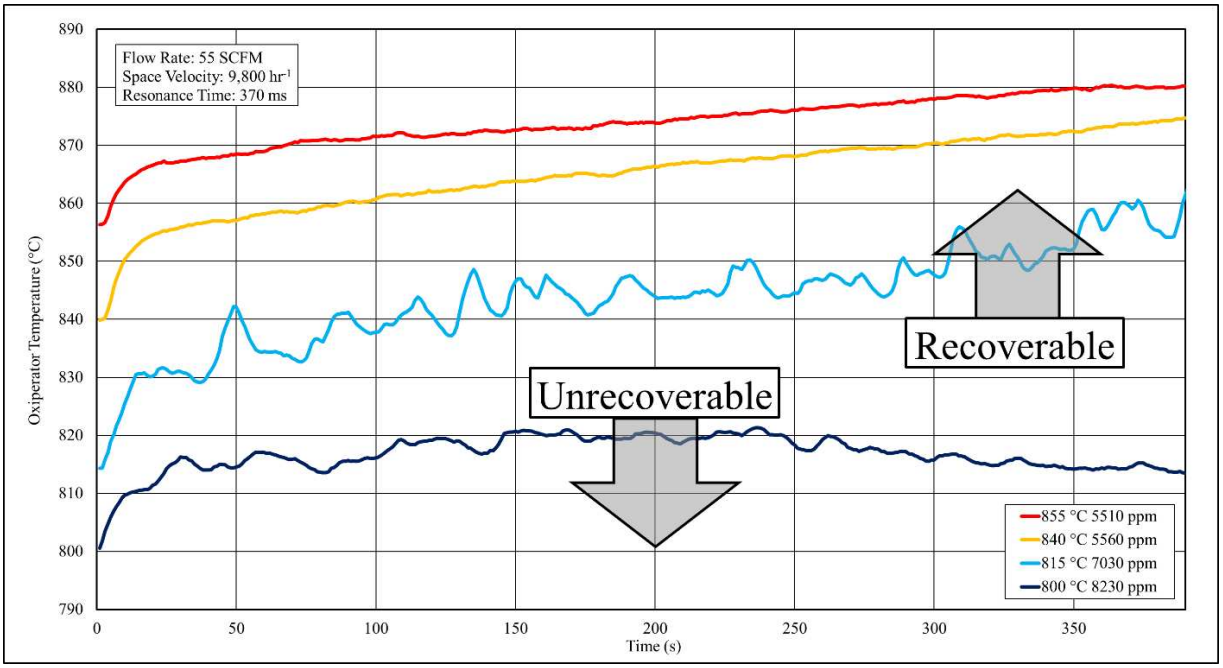

Figure 24: Temperature of Oxiperator after additional natural gas was added during cool off, the legend includes the THC inlet concentration for each temperature

At 855 °C and 840 °C, when the supplementary natural gas was added, the temperature of the Oxiperator immediately increased, and the THC reduction efficiency remained steady at nearly 100%. For the test at 815 °C, the temperature increased, but it was not steady. Additionally, the THC reduction efficiency dropped, but eventually recovered. For the test at 800 °C, when the supplementary natural gas was turned on, the temperature did spike, However, the THC reduction efficiency dropped significantly, and the temperature began to drop again after a few minutes. The

supplementary natural gas was increased to where the concentration of THC reached 8230 ppm and the reaction did not recover. No matter how much natural gas was added, the reaction was not recoverable. It was determined that 815 °C is the lowest temperature the Oxiperator can reach where the reaction is still recoverable.

3.2.3 Temperature Decay

After the temperature recovery test was completed, the supplementary natural gas in the exhaust was completely shut off and the Oxiperator was allowed to slowly cool. During this process, the emissions data of the gas going into and out of the Oxiperator continued to be measured. Figures 25 and 26 show the reduction efficiencies of several different key species as the device cooled. The efficiency lines in both figures are based on trendlines from emissions data at the inlet and outlet of the Oxiperator. This was done to create continuous data lines, as the raw data does not create continuous data due to the sample line only measuring either the inlet or outlet data at any given time. FTIR data used for these figures are averaged and summarized in Appendix D for each inlet and outlet sample period. The Oxiperator did not show any significant reduction in NO_X. This could be a result of the high amount of NO_X being released by the engine. During the temperature decay test, the average incoming NO_X was 4668 ppm and the average outgoing NO_X was 4637 ppm.

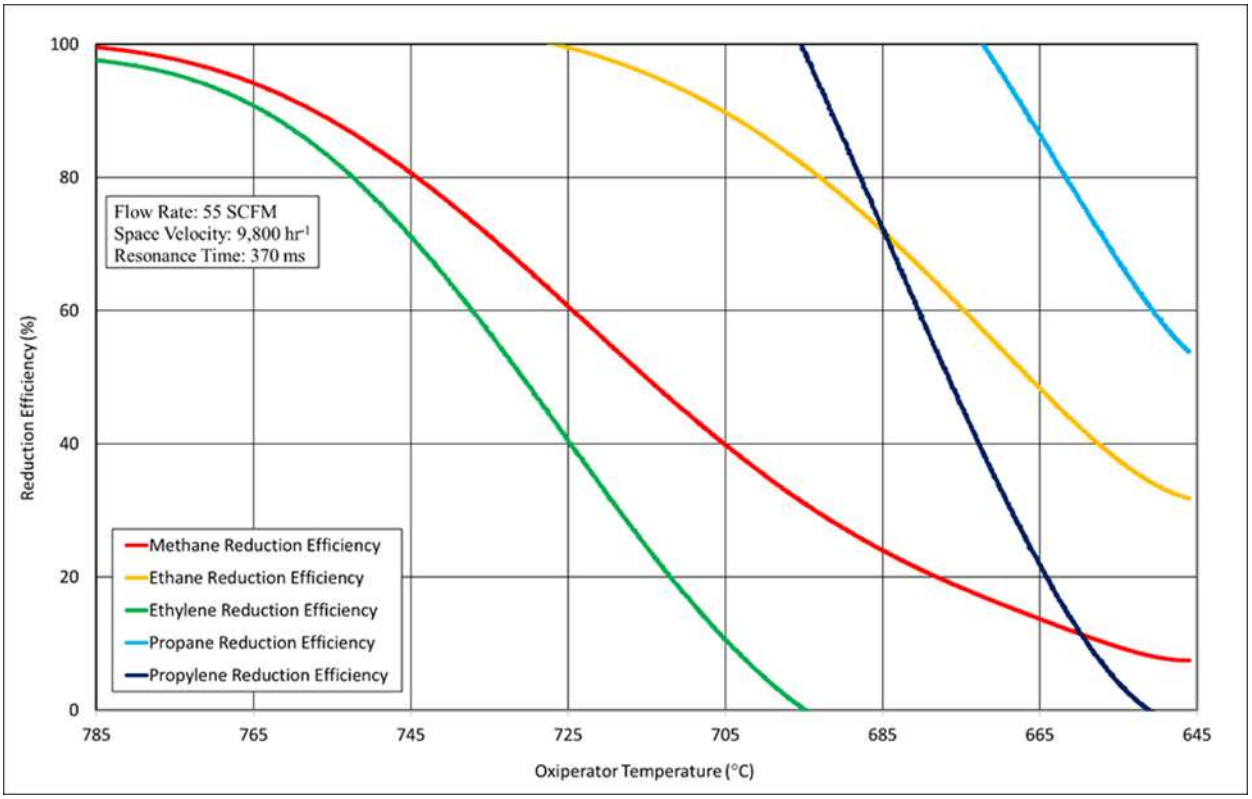

Figure 25: Reduction efficiency of different common hydrocarbons in the exhaust

As the Oxiperator cooled off, the reduction efficiencies of hydrocarbons reduced significantly by the time the device reached 645 °C. The reduction efficiency of Ethane remains higher than the reduction efficiency Ethylene at lower temperatures. Similarly, the reduction efficiency of Propane remains higher than the reduction efficiency of Propylene at lower temperatures. This is significant because for traditional catalytic oxidizers, the trend is the opposite. Commercially available catalysts have been tested on a Waukesha VGF-18 GL lean burn natural gas engine as well as the Cummins QSK19G engine during previous studies at Colorado State University. During these studies, propylene and ethylene reduction efficiency reached above 90% while the propane and ethane reduction efficiency peaked at 30% [49,50].

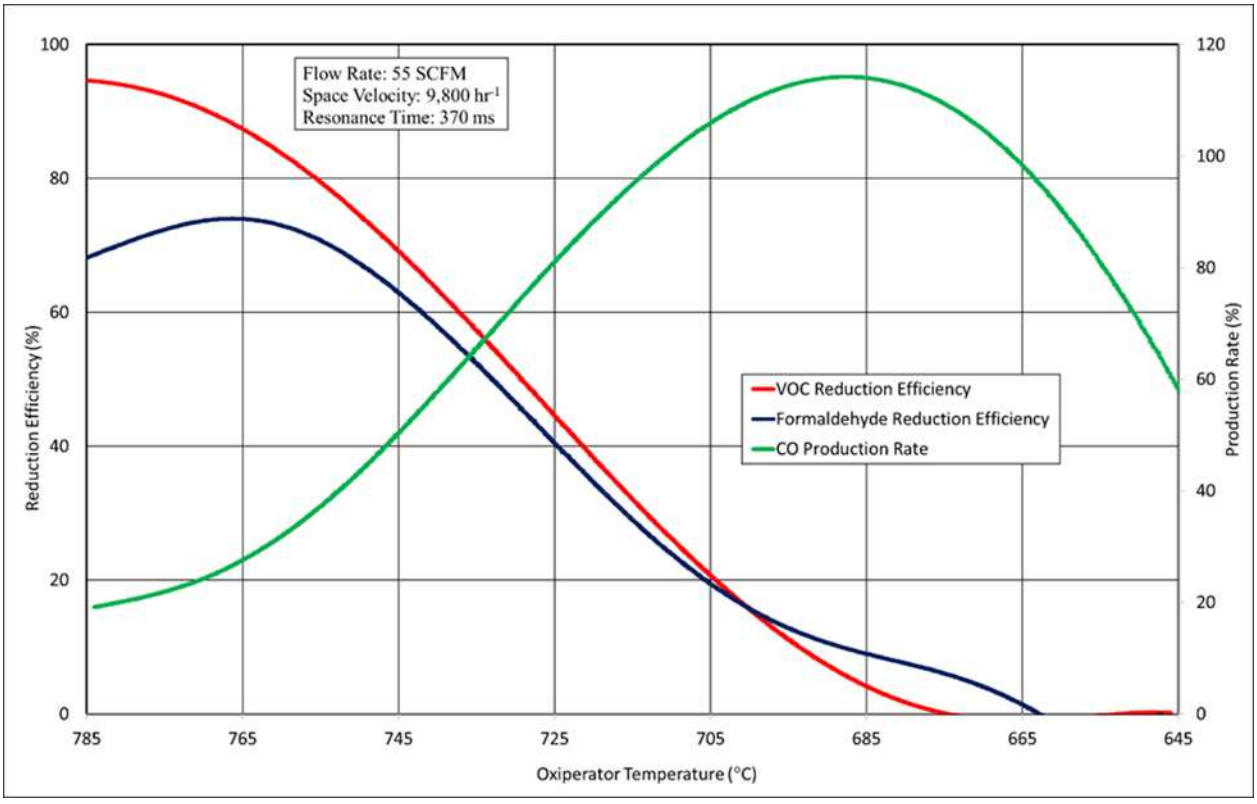

Figure 26: Reduction of VOC and Formaldehyde as well as the CO production rate of the Oxiperator

The rate of CO production increased to a maximum value of 115% at 685 °C before beginning to reduce as the reaction slowed down. The reduction efficiencies of both Formaldehyde and VOC reached 0% by the time that the Oxiperator reached 685 °C.

Table 4 shows the light off temperature of several key species from the Oxiperator test. Light off temperature is defined as the temperature at which a catalytic reaction reaches a conversion efficiency reaches 50% [51]. In this case, with no catalyst present, the light-off temperature is just the temperature at which the species reduction reaches 50% efficiency.

Table 4: Light off temperatures of key hydrocarbons and regulated species. Note: the reduction efficiency of Propane only reached as low as 53.8% at the time of shut off with the temperature being 646 (℃).

Species	Light off Temperatures (°C)
Methane	715
Ethane	666
Ethylene	731
Propane	>646
Propylene	677
VOC	729
Formaldehyde	733

In the catalytic Oxidizer studies performed at Colorado State, the light off temperatures of many of these species were significantly lower than the light off temperatures using the Oxiperator. The light off temperature for VOC in catalytic oxidizers was around 200 °C and 235 °C, much lower than the 729 °C seen in the Oxidizer. In catalytic oxidizers, the light temperatures for Ethylene, Propylene, and Formaldehyde all ranged between 200 °C and 300 °C, depending on the catalyst. In comparison, the light off temperatures for those species in the Oxiperator ranged from 660 °C up to 730 °C. The highest light off temperature seen in the catalytic oxidizer studies was propane, with a light off temperature of 410 °C, still much lower than the 640 °C in the Oxiperator [49,50].

3.2.4 Percentage of Engine Fuel Flow

The amount of fuel required to heat the reactor portion of the reactor relative to the fuel flow to the engine is shown in Figure 27. The key data points for both the minimum THC concentration test and minimum recoverable temperature test are highlighted. This is assuming that the Oxiperator has been scaled up to treat the entire exhaust flow of the engine, not just 50 scfm like during testing. This shows that 5% additional natural gas would be consumed by the system at the minimum THC concentration point. Additionally, a 9% increase of natural gas would be required during temperature recovery.

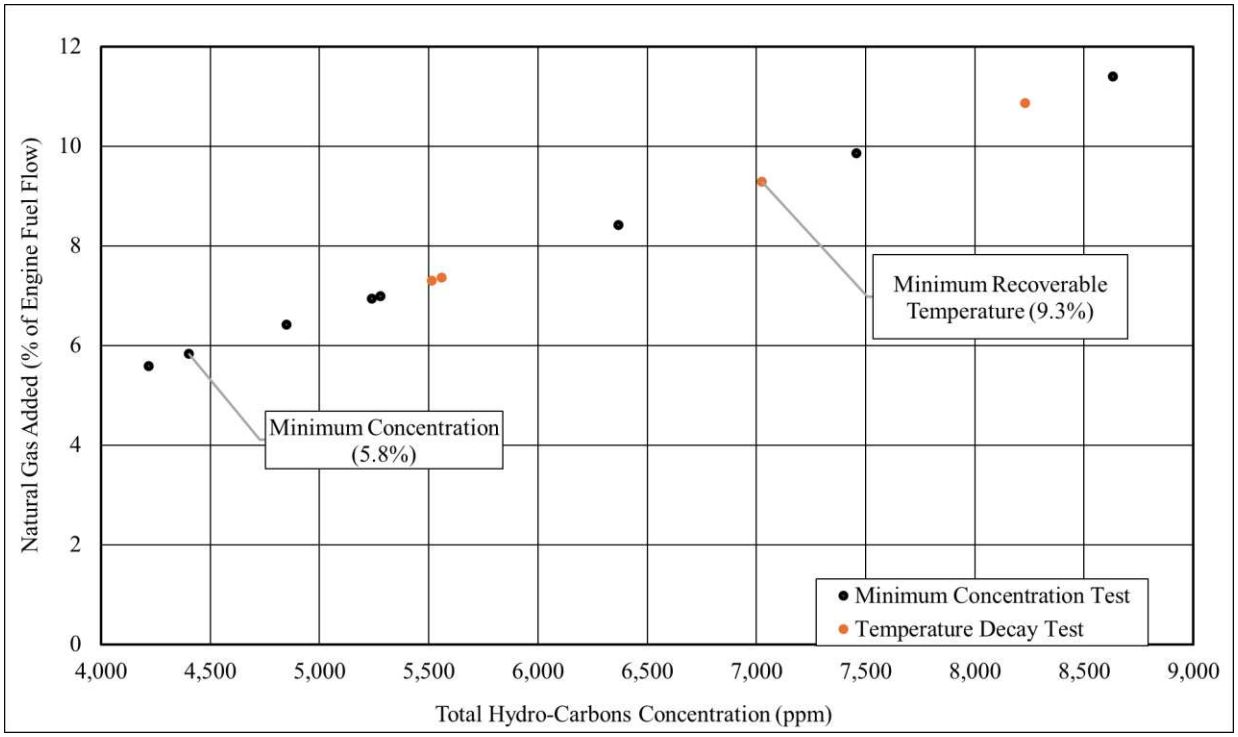

Figure 27: Natural gas required in terms of percentage of engine fuel flow to reach key THC concentrations in the exhaust

3.2.5 Oxiperator Effectiveness

The Bosal P5-100 heat exchanger that is used as the recuperator in the Oxiperator has a rated effectiveness (ϵ) of 82% [52]. The actual effectiveness was calculated using the following equation 2 [53].

$$\epsilon = \frac{T\_hot\_in - T\_hot\_out}{T\_hot\_in - T\_cold\_in} \qquad (2)$$

From Figure 22, T_hot_in is the inlet of the hot side of the recuperator (TC_592), T_hot_out is the outlet of the hot side of the recuperator (TC_780), and T_cold_in is the inlet of the cold side of the recuperator (TC_160). Table 5 summarizes the average recuperator effectiveness during each of the three primary Oxiperator tests.

Table 5: Summary of Oxiperator recuperator effectiveness during testing

Test	**Recuperator Effectiveness (ϵ)**
Minimum THC Concentration	80.9%
Minimum Recoverable Temperature	80.1%
Temperature Decay	80.6%

The recuperator averaged above 80% effectiveness during all three tests. With a rated effectiveness of 82% this specific heat exchanger could not perform significantly better. Generally, the effectiveness of heat exchangers ranges from 50%-80% [54]. This leaves little room for improvement on the recuperator performance.

4. COMPUTER SIMULATION OF SUBSCALE OXIPERATOR

4.1 Simplifying the Model

The Oxiperator consists of dozens of horizontal channels in both the reactor side and the recuperator side. To simplify the model for CONVERGE, the Oxiperator was scaled down to the minimum number of channels, as seen in Figure 28. This results in there being one inlet and one outlet channel on the recuperator side, and two inlet and two outlet channels on the reactor side, due to the reactor channels being half as wide as the recuperator channels.

To improve simulation time, the model did not simulate the solid portion of the Oxiperator. The walls were assumed to be at temperature and were adjusted.

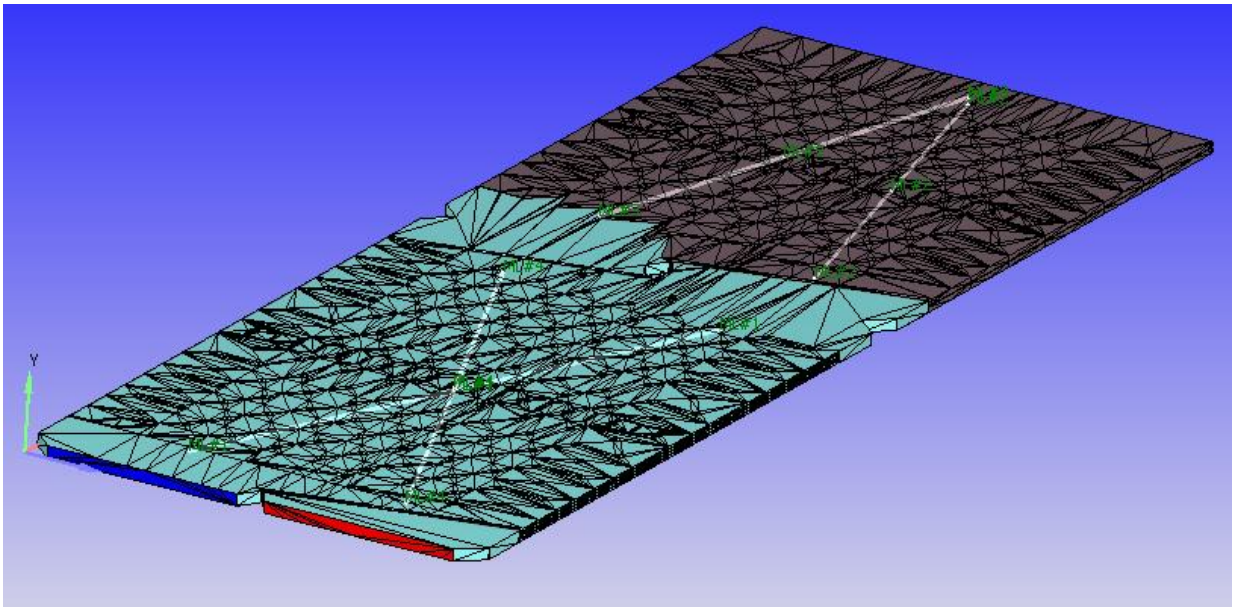

Figure 28: CONVERGE CFD model of Initial Oxiperator

4.2 Heat up Simulation

The first set of simulations was to determine what temperature the exhaust needs to be in order for the methane reacts. The wall temperature of the recuperator was kept constant at 800 K throughout the simulation. This is hotter than the exhaust inlet temperature to simulate the recuperating effect. The reactor wall temperature begins at 800 K and after the flow through the device becomes consistent, it starts to increase.

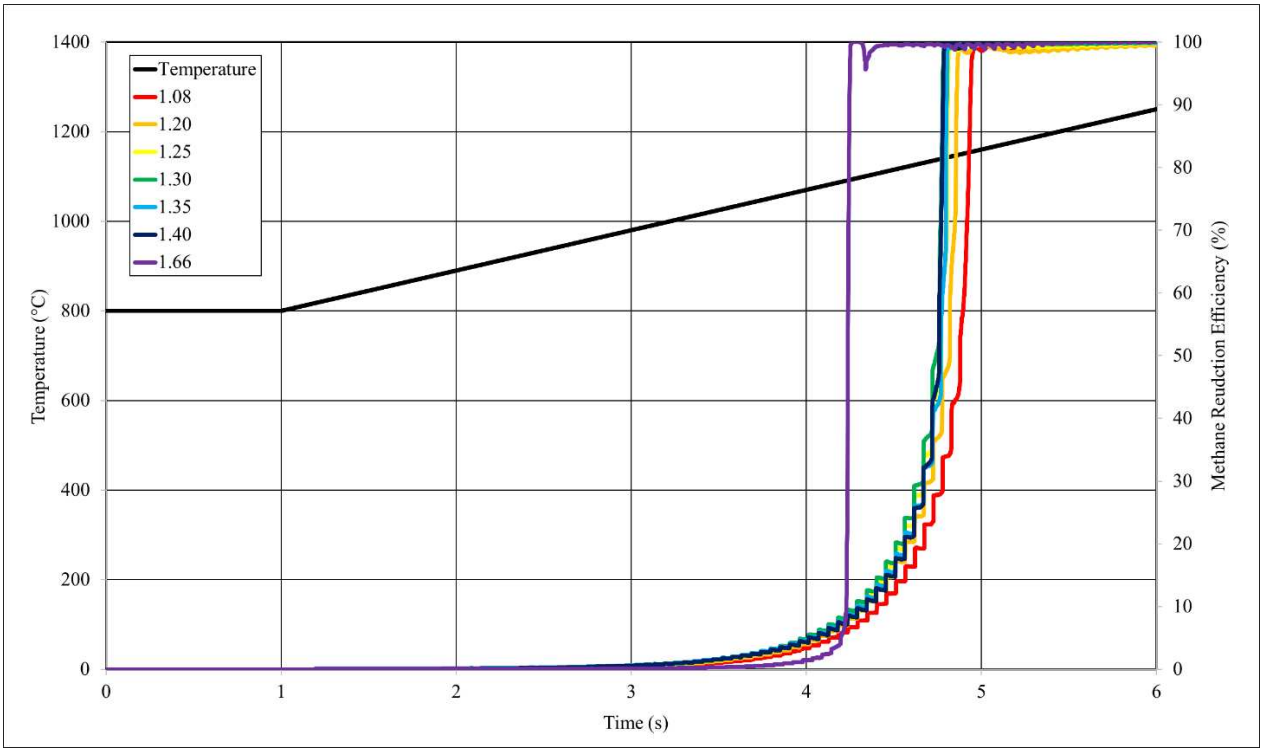

Figure 29: CONVERGE simulation heat up results

Table 6 shown below summarizes the light off temperature at each lambda value. Light off temperature is defined as the temperature at which a catalytic reaction reaches a conversion efficiency reaches 50% [51]. In this case, with no catalyst present, the light-off temperature is just the temperature at which the methane reduction reaches 50% efficiency.

Table 6: Light off temperature of methane inside the reactor portion of the Oxiperator at different lambda values from the CONVERGE CFD simulation.

Lambda	**Light-off Temperature (°C)**
1.08	876.3
1.20	871.0
1.25	866.5
1.30	864.1
1.35	866.3
1.40	865.4

Methane light off temperatures predicted by CONVERGE range between 864 °C and 876 °C. This is higher than the actual Methane light off temperature of the final Oxiperator design which was 715 °C.

4.3 Cool off Simulation

The second set of simulations was set up to simulate the device heating up using a combustor, with the combustor then being shut off. This simulation begins the same as the heat up simulation, but with the reactor wall temperature levelling off at 1200 K. This temperature was picked since the heat up simulation showed that all six lambda values had near 100% methane

reduction at 1200 K. After five seconds at 1200 K, the reactor wall temperature was sent to drop back down to the initial temperature.

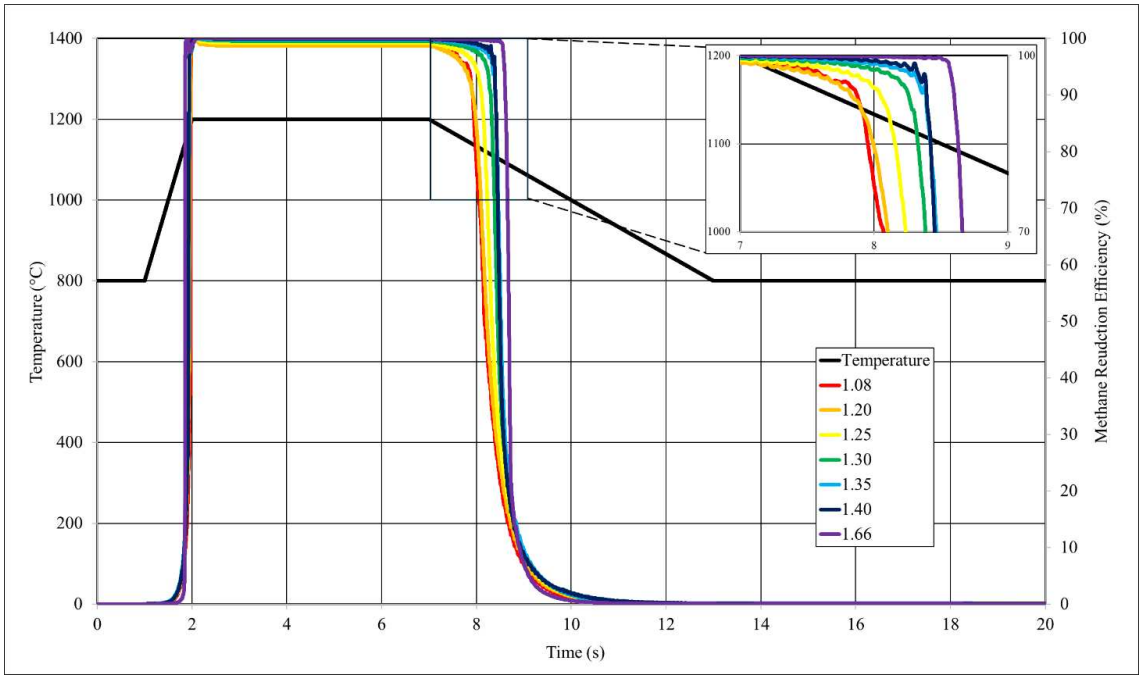

Figure 30: CONVERGE simulation Cool off results

The simulation was not able to sustain a reaction at any of the lambda values. Comparing this to the experimental results of the Oxiperator, the Oxiperator was unable to maintain oxidation at such low THC concentrations in the exhaust. Additional natural gas had to be added to the exhaust to get the Oxiperator to sustain the oxidation reaction and maintain temperatures.

4.4 Final Oxiperator CONVERGE Simulation

Using temperature and emissions data obtained from the Oxiperator test on the engine, a simple CONVERGE simulation was set up using the new Oxiperator design. This was done to compare test data to predictive models. Due to the significantly simpler design of the final Oxiperator, the entire reactor portion of the device was able to be modeled in CONVERGE, seen in Figure 31.

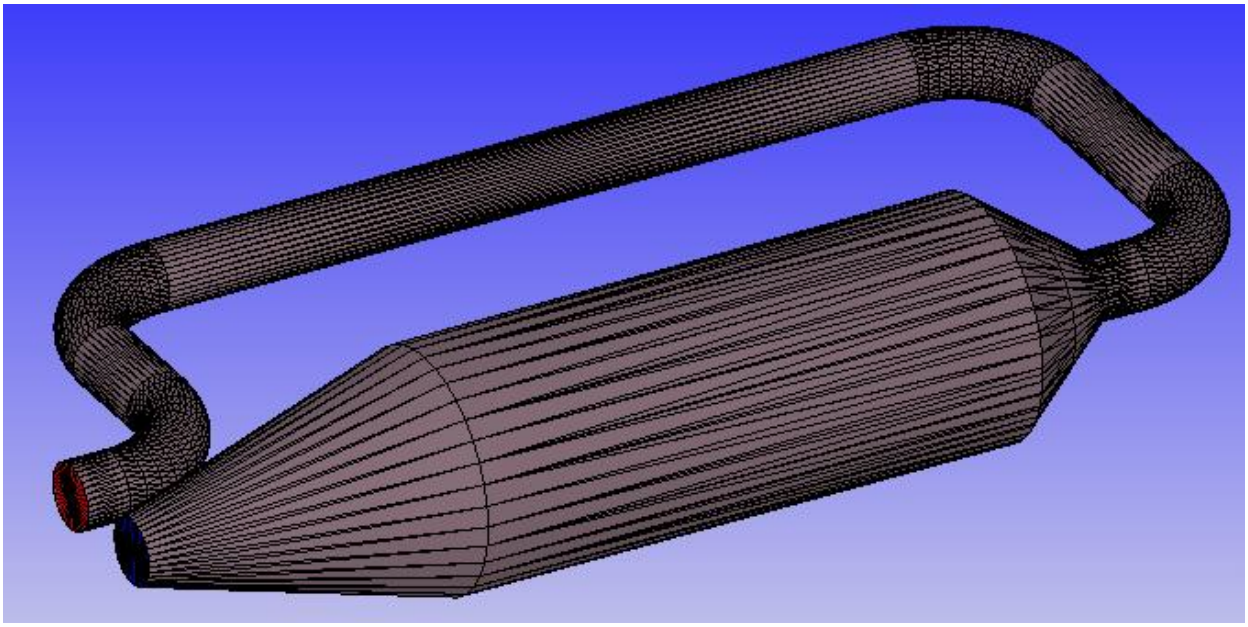

Figure 31: CONVERGE CFD model of the Final Oxiperator

For the final Oxiperator simulation, the gas was set to match the same composition of the 4400-ppm set point of the minimum concentration test. The gas composition is summarized in Table 7. The gas temperature and wall temperature were set to the average Oxiperator temperature

during the Oxiperator test which was 800 K. The wall temperature was increased up to 1200 K to induce Oxidation and was then decreased back to 800 K.

Table 7: Exhaust Concentration for Final Oxiperator Simulation

Species	Concentration
N_2	71.09 %
CO_2	13.32 %
H_2O	12.27 %
O_2	2.549 %
NO	4890 ppm
CH_4	1907 ppm
C_2H_6	377 ppm
CO	278 ppm
C_3H_8	55 ppm
CH_2O	42 ppm
C_2H_4	30 ppm
C_2H_2	~3 ppm
CH_3OH	~2 ppm
N_2O	~1 ppm
NH_3	>1 ppm

Unlike the simulations made on the initial Oxiperator design model, there were steady state conditions. Figure 32 shows the overall concentration of Methane in the model as well as the temperature of the wall throughout the twenty second simulation.

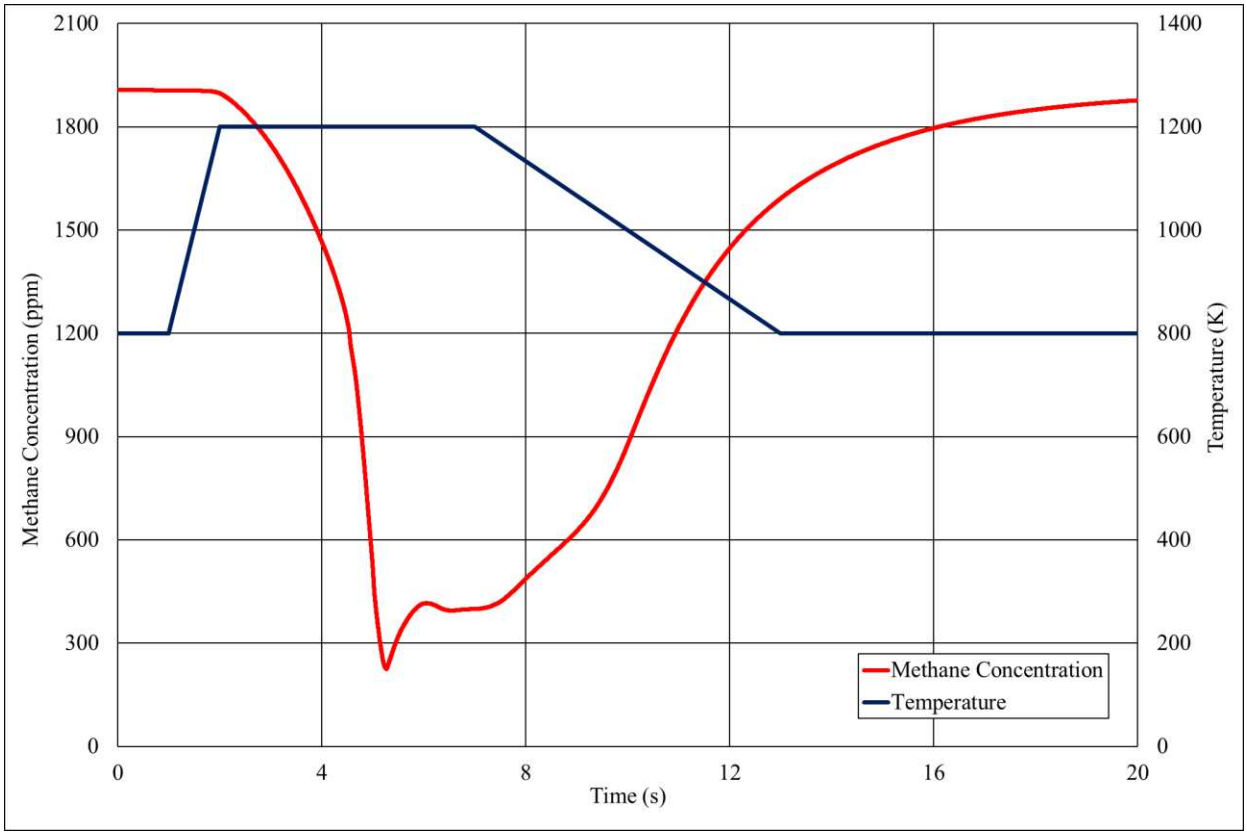

Figure 32: Change of Methane Concentration and wall temperature during the Final Oxiperator Simulation, the incoming gas was set at 800 K with a THC concentration of 4400 ppm

The reaction begins and the concentration of Methane reduces significantly, reaching a minimum of 250 ppm at around the five second mark. After that, the reaction does not sustain as the temperature decreases back to its starting value. Methane concentration rises back to its starting value. Comparing this simulation and the results shown in Figure 32 to the actual test of the Oxiperator, we can see that the actual test showed different results. At these conditions, the Oxiperator was able to maintain oxidation and was able sustain temperatures without losing heat. This simulation showed a brief moment of oxidation, but did not sustain as seen in the actual test.

5. SUMMARY AND CONCLUSION

A thermal oxidizer, coined an Oxiperator, was evaluated on its ability to reduce THC emissions from a lean burn natural gas engine and what conditions were required to do so. A baseline test was performed on the selected engine, a Cummins QSK19G lean burn natural gas engine, to determine the optimal operating condition for the Oxiperator. The Oxiperator was then tested on the QSK19G engine, and three primary tests were performed, with the first being to determine the minimum THC concentration required to maintain Oxiperator temperature. Another test was conducted to determine what is the coldest the Oxiperator can get where the reaction can be recovered. Finally, a third test was performed to analyze the oxidation efficiency of the Oxiperator as it cools. Additionally, CONVERGE CFD was evaluated on its ability to accurately predict the performance of a thermal oxidizer. This was done by comparing the test results of the Oxiperator to a computer simulated model of the Oxiperator.

The primary takeaway from the initial baseline test of the Cummins QSK19G is that a leaner air fuel ratio is better for Oxiperator testing. The Oxiperator requires a substantial amount of THC in the exhaust to maintain operation. As the air fuel ratio of the engine became leaner, the concentration of THC increased in the exhaust. However, due to complications of the engine controls, the engine was unable to operate at the same speed and air fuel ratio as it was during the baseline test. It may be beneficial for the Altronic Controls to be replaced out for the original Cummins control. For future testing involving the Cummins QSK19G, controls will need to be reworked.

The Oxiperator required a minimum THC concentration of 4400 ppm to sustain operation temperature. At any concentration lower than 4400 ppm, the Oxiperator temperature decreased and

would eventually stop the oxidation of hydrocarbons. 815 °C is the lowest temperature that the Oxiperator can reach before the reaction becomes unrecoverable. At temperatures below 815 °C, adding additional methane to the inlet of the Oxiperator does not recover the temperature. Even with a THC concentration of 8000 ppm, the Oxiperator was unable to recover at 800 °C. During cooldown, the reduction efficiencies of all major hydrocarbons trailed off as the Oxiperator temperature reached 650 °C. Notably, the reduction efficiency of propylene and ethylene dropped at higher temperatures than propane and ethane. This is the opposite trend as what happens when using catalytic oxidizers. The light off temperatures of these significant species in the Oxiperator were substantially greater when compared to catalytic oxidizers. Catalytic oxidizers have light off temperatures in the range of 200-400 °C, while the Oxiperator had temperatures ranging from 650-750 °C.

The first CONVERGE CFD simulation was a heat up simulation predicting light off temperatures of methane using the initial Oxiperator design. The CONVERGE simulation predicted light off temperatures for methane around 870 °C and multiple different air fuel ratios. The actual methane light off temperature in the Oxiperator was 715 °C. Considering the CONVERGE model used in this simulation did not end up matching the actual model tested, more simulations would need to be run to determine the viability. The next CONVERGE simulation performed was a cooldown test, using the initial Oxiperator design, to determine if the Oxiperator would be able to maintain temperature at different THC concentrations in the exhaust. The simulation predicted that the Oxiperator would not be able to maintain temperature with just the THC present in the exhaust. This matches the live Oxiperator test, as additional natural gas was required to be added to the exhaust, up to a concentration of 4400 THC, to maintain temperature. The final CONVERGE simulation, using the final Oxiperator design, used the same conditions as

the successful Oxiperator performance test. The simulation predicted that the Oxiperator would not sustain methane reduction, opposing the results of the performance test. CONVERGE CFD was successful in predicting certain aspects of the Oxiperator performance but failing in others. To determine whether or not CONVERGE CFD could be a useful tool in predicting the performance of thermal oxidizers, more models and simulations would need to be performed.

For the next design of the Oxiperator, there are several improvements that could be made. First, a premixed combustor could be used in place of the current one. The current combustor requires significantly more air than is present natural gas engine exhaust. This meant that, as soon as the flow was switched to the engine exhaust, the combustor was unable to relight. With a premixed combustor, it would be able to reheat the Oxiperator even after the flow had been switched over. Additionally, redesigning how the Oxiperator is thermally insulated could improve its utility. The current design requires a large container surrounding the Oxiperator to be filled with thermal powder. This makes the Oxiperator to be very inaccessible, meaning that replacing probes and checking connections required substantial work, as the thermal powder had to be removed to make the Oxiperator accessible. This also made the device quite heavy and hard to maneuver in the lab. A design that uses thermal insulation that could be wrapped around the Oxiperator would make it significantly lighter, as well as make it more accessible.

REFERENCES

1. US EPA, O. Overview of Greenhouse Gases Available online: https://www.epa.gov/ghgemissions/overview-greenhouse-gases (accessed on 8 February 2024).

2. US EPA, O. Inventory of U.S. Greenhouse Gas Emissions and Sinks: 1990-2020 Available online: https://www.epa.gov/ghgemissions/inventory-us-greenhouse-gas-emissions-and-sinks-1990-2020 (accessed on 8 February 2024).

3. US EPA, O. Importance of Methane Available online: https://www.epa.gov/gmi/importance-methane (accessed on 8 February 2024).

4. Methane and Climate Change – Global Methane Tracker 2022 – Analysis Available online: https://www.iea.org/reports/global-methane-tracker-2022/methane-and-climate-change (accessed on 8 February 2024).

5. Background NaturalGas.Org. Available online: https://naturalgas.org/overview/background (accessed on 9 February 2024).

6. Use of Natural Gas - U.S. Energy Information Administration (EIA) Available online: https://www.eia.gov/energyexplained/natural-gas/use-of-natural-gas.php (accessed on 8 February 2024).

7. Preliminary Monthly Electric Generator Inventory (Based on Form EIA-860M as a Supplement to Form EIA-860) - U.S. Energy Information Administration (EIA) Available online: https://www.eia.gov/electricity/data/eia860m/index.php (accessed on 8 February 2024).

8. EIA - Natural Gas Pipeline Network - Transporting Natural Gas in the United States Available online: https://www.eia.gov/naturalgas/archive/analysis_publications/ngpipeline/index.html (accessed on 8 February 2024).

9. CIMAC WG17 | Methane and Formaldehyde Emissions of Gas Engines Available online: //www.cimac.com/publications/publications350/cimac-wg17-methane-and-formaldehyde-emissions-of-gas-engines.html (accessed on 8 February 2024).

10. Vaughn, T.L.; Luck, B.; Williams, L.; Marchese, A.J.; Zimmerle, D. Methane Exhaust Measurements at Gathering Compressor Stations in the United States. *Environ. Sci. Technol.* **2021**, *55*, 1190–1196, doi:10.1021/acs.est.0c05492.

11. Learn About the Greenhouse Gas Reporting Program (GHGRP) | Greenhouse Gas Reporting Program (GHGRP) | US EPA Available online: https://climatechange.chicago.gov/ghgreporting/learn-about-greenhouse-gas-reporting-program-ghgrp (accessed on 8 February 2024).

12. US EPA, O. Subpart W – Petroleum and Natural Gas Systems Available online: https://www.epa.gov/ghgreporting/subpart-w-petroleum-and-natural-gas-systems (accessed on 8 February 2024).

13. US EPA, O. Methane Emissions Reduction Program Available online: https://www.epa.gov/inflation-reduction-act/methane-emissions-reduction-program (accessed on 8 February 2024).

14. US EPA, O. EPA Proposes to Strengthen Air Quality Standards to Protect the Public from Harmful Effects of Soot Available online: https://www.epa.gov/newsreleases/epa-proposes-strengthen-air-quality-standards-protect-public-harmful-effects-soot (accessed on 8 February 2024).

15. 40 CFR Part 60 Subpart JJJJ -- Standards of Performance for Stationary Spark Ignition Internal Combustion Engines Available online: https://www.ecfr.gov/current/title-40/part-60/subpart-JJJJ (accessed on 8 February 2024).

16. US EPA, O. What Is the Definition of VOC? Available online: https://www.epa.gov/air-emissions-inventories/what-definition-voc (accessed on 8 February 2024).

17. Lindblom, J.; Su, W. Methane Slip Prevention in the Combustion Chamber, Chalmers University of Technology: Goteborg, Swedne, 2021.

18. Jensen, M.V.; Cordtz, R.F.; Schramm, J. Numerical Analysis of Methane Slip Source Distribution in a Four-Stroke Dual-Fuel Marine Engine. *J Mar Sci Technol* **2021**, *26*, 606–617, doi:10.1007/s00773-020-00760-3.

19. Castillo, A.Q.; Zdanowicz, A.; Windom, B.; Olsen, D. Characterization of Crankcase Ventilation Gas on Stationary Natural Gas Engines. In Proceedings of the Alternative Fuels and Emissions; College Station, Texas, March 19 2023.

20. Hiltner, J. Unburned Hydrocarbon Emissions from Lean Burn Natural Gas Engines – Sources and Solutions. **2016**.

21. Huonder, A.; Olsen, D. Methane Emission Reduction Technologies for Natural Gas Engines: A Review. *Energies* **2023**, *16*, 7054, doi:10.3390/en16207054.

22. Innovative Environmental Solutions, Inc. &; Optimized Technical Solutions *Availability and Limitations of NOx Emission Control Resources for Natural Gas-Fired Reciprocating Engine Prime Movers Used in the Interstate Natural Gas Transmission Industry*; The INGAA Foundation, Inc, 2014;

23. Hampson, G.J. High Efficiency Natural Gas Engine Combustion Using Controlled Auto-Ignition. In Proceedings of the ASME 2019 Internal Combustion Engine Division Fall Technical Conference; American Society of Mechanical Engineers: Chicago, Illinois, USA, October 20 2019; p. V001T03A019.

24. Vieira, G.; Beurlot, K.; Xie, N.; Patterson, M.; Olsen, D. Pre-Combustion Chamber Nozzle Design Effect on Unburned Methane Emissions of a Large Bore Two-Stroke Lean- Burn Natural Gas Engine.

25. Olsen, D.B.; Willson, B.D. The Effect of Retrofit Technologies on Formaldehyde Emissions from a Large Bore Natural Gas Engine. *EPE* **2011**, *03*, 574–579, doi:10.4236/epe.2011.34071.

26. Pio Forzatti; Luca Lietti Catalyst Deactivation. *Catalysis Today* **1999**, 165–181, doi:doi:10.1016/S0920-5861(99)00074-7.

27. Gélin, P.; Primet, M. Complete Oxidation of Methane at Low Temperature over Noble Metal Based Catalysts: A Review. *Applied Catalysis B: Environmental* **2002**, *39*, 1–37, doi:10.1016/S0926-3373(02)00076-0.

28. Zhang, Y.; Glarborg, P.; Johansen, K.; Andersson, M.P.; Torp, T.K.; Jensen, A.D.; Christensen, J.M. A Rhodium-Based Methane Oxidation Catalyst with High Tolerance to H2O and SO2. *ACS Catal.* **2020**, *10*, 1821–1827, doi:10.1021/acscatal.9b04464.

29. Daniel Olsen; Walter Hull; Patrick Ginger; Colin Olson; Bryan Willson *Humidity Control for Power and Emissions; Gas Research Institute*; Gas Research Institute, 2002;

30. Defoort, M.; Olsen, D.; Willson, B. Performance Evaluation of Oxidation Catalysts for Natural Gas Reciprocating Engines.

31. Hopoko *Test Report on Exhaust Emissions from One Solar Mars T-1200 Gas Turbine, Four Cooper Bessemer GMVA-10 Engines, Eight Copper Messemer GMV-10 Engines, and Five Ingersol Rand KVS-12 Engines at the Holbrook Compressor Station; Division of Technical Services and Monitoring Bureau of Air Quality Control*;

32. Yamamoto, H.; Uchida, H. Oxidation of Methane over Pt and Pd Supported on Alumina in Lean-Burn Natural-Gas Engine Exhaust. *Catalysis Today* **1998**, *45*, 147–151, doi:10.1016/S0920-5861(98)00265-X.

33. Worth, D.J.; Stettler, M.E.J.; Dickinson, P.; Hegarty, K.; Boies, A.M. Characterization and Evaluation of Methane Oxidation Catalysts for Dual-Fuel Diesel and Natural Gas Engines. *Emiss. Control Sci. Technol.* **2016**, *2*, 204–214, doi:10.1007/s40825-016-0047-x.

34. Abbasi, R.; Huang, G.; Istratescu, G.M.; Wu, L.; Hayes, R.E. Methane Oxidation over Pt, Pt:Pd, and Pd Based Catalysts: Effects of Pre-treatment. *Can J Chem Eng* **2015**, *93*, 1474–1482, doi:10.1002/cjce.22229.

35. Gremminger, A.; Pihl, J.; Casapu, M.; Grunwaldt, J.-D.; Toops, T.J.; Deutschmann, O. PGM Based Catalysts for Exhaust-Gas after-Treatment under Typical Diesel, Gasoline and Gas Engine Conditions with Focus on Methane and Formaldehyde Oxidation. *Applied Catalysis B: Environmental* **2020**, *265*, 118571, doi:10.1016/j.apcatb.2019.118571.

36. Caravaggio, G.; Nossova, L.; Turnbull, M.J. Nickel-Magnesium Mixed Oxide Catalyst for Low Temperature Methane Oxidation. *Chemical Engineering Journal* **2021**, *405*, 126862, doi:10.1016/j.cej.2020.126862.

37. Amelio, M.; Morrone, P. Numerical Evaluation of the Energetic Performances of Structured and Random Packed Beds in Regenerative Thermal Oxidizers. *Applied Thermal Engineering* **2007**, *27*, 762–770, doi:10.1016/j.applthermaleng.2006.10.016.

38. Cheng, W.-H.; Chou, M.-S.; Lee, W.-S.; Huang, B.-J. Applications of Low-Temperature Regenerative Thermal Oxidizers to Treat Volatile Organic Compounds. *J. Environ. Eng.* **2002**, *128*, 313–319, doi:10.1061/(ASCE)0733-9372(2002)128:4(313).

39. Li, Q.; Lin, B.; Yuan, D.; Chen, G. Demonstration and Its Validation for Ventilation Air Methane (VAM) Thermal Oxidation and Energy Recovery Project. *Applied Thermal Engineering* **2015**, *90*, 75–85, doi:10.1016/j.applthermaleng.2015.06.089.

40. Liu, R.; Liu, Y.; Gao, Z. Methane Emission Control by Thermal Oxidation in a Reverse Flow Reactor. In Proceedings of the 2008 2nd International Conference on Bioinformatics and Biomedical Engineering; IEEE: Shanghai, May 2008; pp. 3952–3955.

41. Marín, P.; Díez, F.V.; Ordóñez, S. Reverse Flow Reactors as Sustainable Devices for Performing Exothermic Reactions: Applications and Engineering Aspects. *Chemical Engineering and Processing - Process Intensification* **2019**, *135*, 175–189, doi:10.1016/j.cep.2018.11.019.

42. Liu, B.; Hayes, R.E.; Checkel, M.D.; Zheng, M.; Mirosh, E. Reversing Flow Catalytic Converter for a Natural Gas/Diesel Dual Fuel Engine. *Chemical Engineering Science* **2001**.

43. Bayliff, S.; Marchese, A.; Windom, B.; Olsen, D. The Effect of EGR on Knock Suppression, Efficiency, and Emissions in a Stoichiometric, Spark Ignited, Natural Gas Engine.

44. Qu, J.; Feng, Y.; Xu, G.; Zhang, M.; Zhu, Y.; Zhou, S. Design and Thermodynamics Analysis of Marine Dual Fuel Low Speed Engine with Methane Reforming Integrated High Pressure Exhaust Gas Recirculation System. *Fuel* **2022**, *319*, 123747, doi:10.1016/j.fuel.2022.123747.

45. Robinson, C.; Smith, D.B. The Auto-Ignition Temperature of Methane. *Journal of Hazardous Materials* **1984**, *8*, 199–203, doi:10.1016/0304-3894(84)85001-3.

46. FREEFLOW® Pourable Insulation for Complex Shapes and Cavities Available online: https://www.promat.com/en/industry/products-solutions/high-temperature-insulation/pourable-products/freeflow/] (accessed on 8 February 2024).

47. CONVERGE CFD Software Available online: https://convergecfd.com/products/converge-cfd-software (accessed on 8 February 2024).

48. Part 4: Oxygen References Context and Calculations Available online: https://yellowtree.co.za/oxygen-references/ (accessed on 8 February 2024).

49. Badrinarayanan, K. PERFORMANCE EVALUATION OF MULTIPLE OXIDATION CATALYSTS ON A LEAN BURN NATURAL GAS ENGINE.

50. Davis, K. OXIDATION CATALYST DEGRADATION IN THE EXHAUST STREAM OF A LARGE BORE 2-STROKE NATURAL GAS ENGINE.

51. Mahadeven, G.; Sendilvelan, S. Temperature Analysis of Dynamic Catalytic Convertor System with Pre-Catalyst in a Multi Cylinder Spark Ignition Engine to Reduce Light-off Time. *IJHT* **2017**, *35*, 97–102, doi:10.18280/ijht.350113.

52. P5-LPD-100 Available online: https://calculator.eci.bosal.com/products/p5-lpd-100/8 (accessed on 28 March 2025).

53. Guo, Z.Y.; Liu, X.B.; Tao, W.Q.; Shah, R.K. Effectiveness–Thermal Resistance Method for Heat Exchanger Design and Analysis. *International Journal of Heat and Mass Transfer* **2010**, *53*, 2877–2884, doi:10.1016/j.ijheatmasstransfer.2010.02.008.

54. Flat Plate Heat Exchanger - an Overview | ScienceDirect Topics Available online: https://www.sciencedirect.com/topics/engineering/flat-plate-heat-exchanger (accessed on 28 March 2025).

APPENDIX A

Catalyst	Ratio	Density (g/m^3)	CH_4 (ppm)	O_2 (%)	H_2O (%)	SO_2 (ppm)	Aged	T(°C)	Conversion (%)	Source
Pd	-	10400	2000	10.5	10	-	No	385	70	[32]
Pd	-	10400	2000	10.5	10	-	1500 hr of use	385	10	[32]
Pd	-	51800	2000	10.5	10	-	No	385	77	[32]
Pd	-	51800	2000	10.5	10	-	1500 hr of use	385	25	[32]
Pt	-	9600	2000	10.5	10	-	No	385	35	[32]
Pt	-	9600	2000	10.5	10	-	1500 hr of use	385	25	[32]
Pt:Pd	1:1	20800	2000	10.5	10	-	No	385	79	[32]
Pt:Pd	1:1	20800	2000	10.5	10	-	1500 hr of use	385	60	[32]
Pt:Pd	2:3	27900	2000	10.5	10	-	No	385	80	[32]
Pt:Pd	2:3	27900	2000	10.5	10	-	1500 hr of use	385	55	[32]
Pt:Pd	1:5	12000	7500	NR	4.89	-	No	325	100	[33]
								300	75	
								300	50	
Pt:Pd	3:41	4400	7500	NR	4.89	-	No	525	100	[33]
								425	75	
								400	50	
Pt:Pd	3:40	4300	7500	NR	4.89	-	No	350	100	[33]
								325	75	
								300	50	
Pt:Pd	10:47	5700	7500	NR	4.89	-	No	375	100	[33]
								350	75	
								325	50	
Pd	-	210	7500	NR	4.89	-	No	N/A	100	[33]
								550	75	
								500	50	
Pd	-	1400	7500	NR	4.89	-	No	450	100	[33]
								400	75	
								350	50	
Pd	-	5297	100000	20	-	-	No	359	75	[34]
								321	50	
								282	25	
Pd	-	5297	100000	20	-	-	Hydrothermally	426	75	[34]
								394	50	
								355	25	
Pd	-	5297	100000	20	5	-	Hydrothermally	492	75	[34]
								452	50	
								421	25	
Pt	-	3355	100000	20	-	-	No	582	75	[34]
								541	50	
								477	25	
Pt	-	3355	100000	20	-	-	Hydrothermally	634	75	[34]
								607	50	
								556	25	
Pt	-	3355	100000	20	5	-	Hydrothermally	632	75	[34]
								604	50	
								557	25	

Pt:Pd	4:10	3355	100000	20	-	-	No	437	75	[34]
								403	50	
								360	25	
Pt:Pd	4:10	3355	100000	20	-	-	Hydrothermally	471	75	[34]
								433	50	
								380	25	
Pt:Pd	4:10	3355	100000	20	5	-	Hydrothermally	548	75	[34]
								497	50	
								455	25	
Pd	-	2260	3000	12	6	-	No	450	100	[35]
								400	75	
								392	50	
Pd	-	2260	3000	12	12	-	No	550	100	[35]
								450	75	
								448	50	
Pd	-	2260	3000	1.5	12	-	No	N/A	50	[35]
Pt	-	2295	3000	12	6	-	No	N/A	50	[35]
Pt	-	2295	3000	12	12	-	No	N/A	50	[35]
Pt	-	2295	3000	1.5	12	-	No	550	100	[35]
								500	75	
								500	50	
Pt:Pd	1:5	2437	3000	12	6	-	No	500	100	[35]
								400	75	
								393	50	
Pt:Pd	1:5	2437	3000	12	12	-	No	500	100	[35]
								435	75	
								427	50	
Pt:Pd	1:5	2437	3000	1.5	12	-	No	N/A	50	[35]
Rh	-	2% wt	2500	10	-	-	No	425	100	[27]
								350	75	
								325	50	
Rh	-	2% wt	2500	10	5	-	No	500	100	[27]
								400	75	
								387	50	
Rh	-	2% wt	2500	10	-	20	No	500	100	[27]
								462	75	
								437	50	
Rh	-	2% wt	2500	10	5	20	No	550	100	[27]
								487	75	
								475	50	
Pd	-	2% wt	2500	10	-	-	No	462	100	[27]
								362	75	
								350	50	
Pd	-	2% wt	2500	10	5	-	No	475	100	[27]
								425	75	
								412	50	
Pd	-	2% wt	2500	10	-	20	No	550	100	[27]
								475	75	
								425	50	
Pd	-	2% wt	2500	10	5	20	No	N/A	100	[27]
								525	75	

								512	50	
Ni:Mg	9:1	6250000	10000	10	10	-	No	550	100	[36]
								500	75	
								480	50	
Ni:Mg	9:1	6250000	10000	10	10	-	40 hr of use	550	100	[36]
								540	75	
								504	50	
Pd	-	1% wt	10000	10	10	-	No	450	100	[36]
								425	75	
								396	50	
Pd	-	1% wt	10000	10	10	-	40 hr of use	575	100	[36]
								540	75	
								507	50	

APPENDIX B

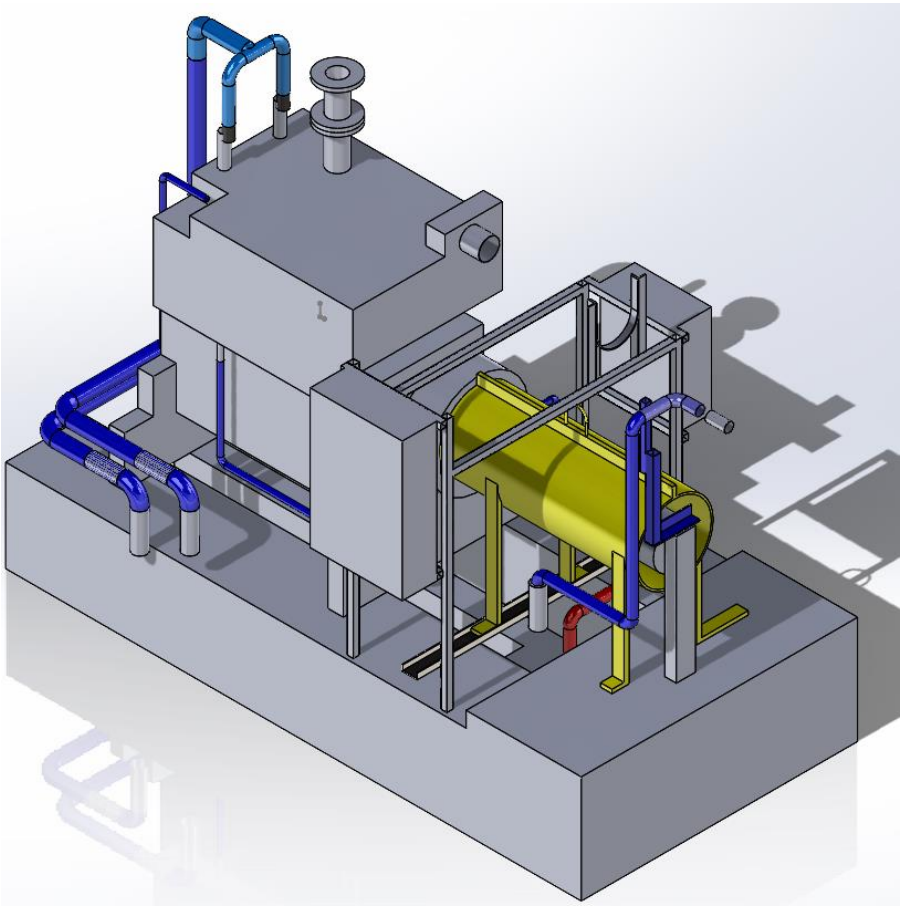

Figure B-1: SolidWorks Model of Cummins QSK19G Piping Layout

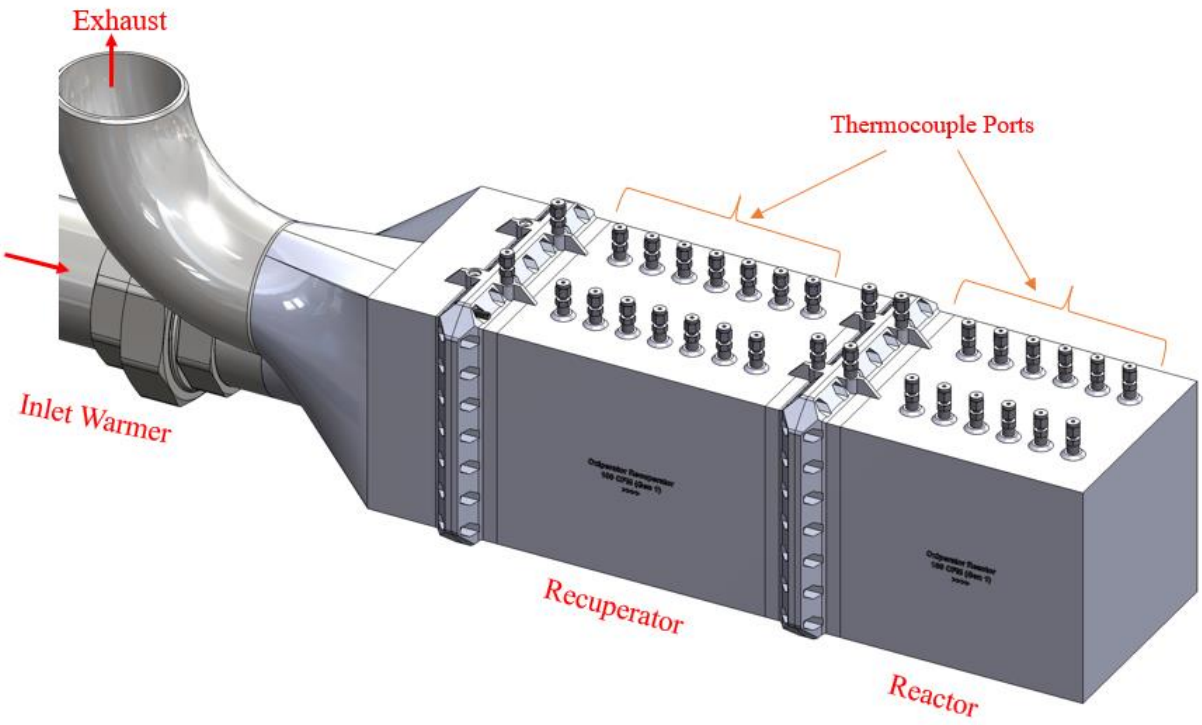

Figure B-2: SolidWorks Model of Initial Oxiperator Design

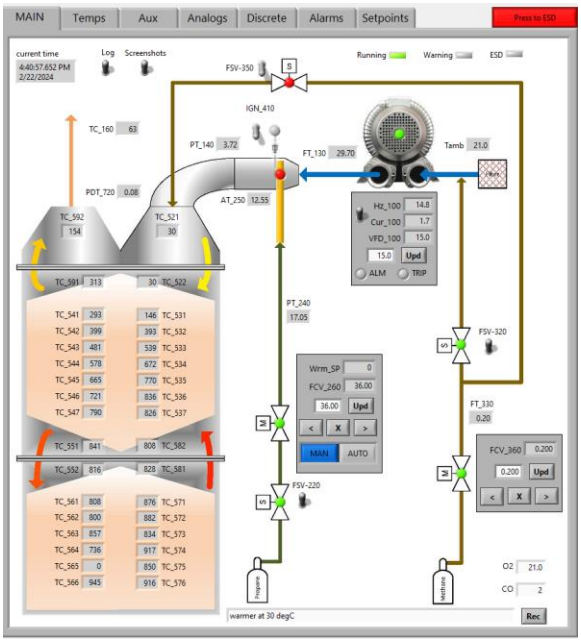

Figure B-3: LabVIEW control panel for Original Oxiperator Bench Test

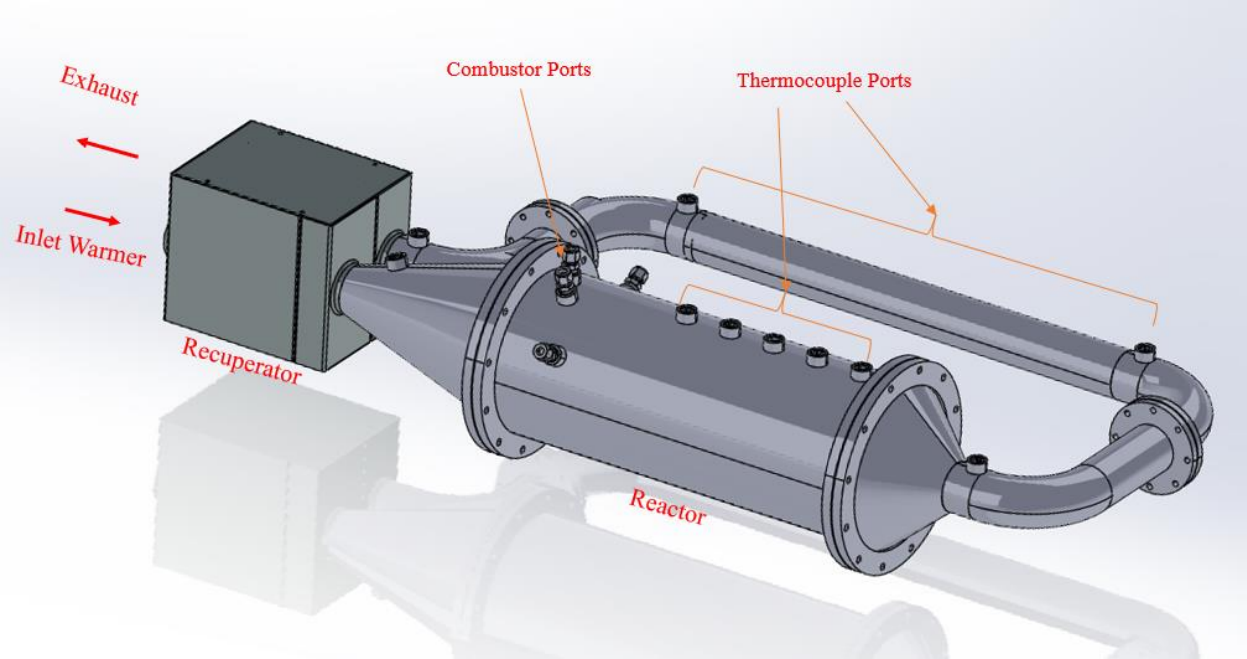

Figure B-4: SolidWorks Model of Final Oxiperator Design

APPENDIX C

Lambda	1.08	1.20	1.25	1.30	1.35	1.40
RPM	1.51E+03	1.51E+03	1.51E+03	1.51E+03	1.51E+03	1.51E+03
Power[hp]	4.02E+02	4.02E+02	4.02E+02	4.02E+02	4.02E+02	4.02E+02
Torque[ft-lb]	1.40E+03	1.40E+03	1.40E+03	1.40E+03	1.40E+03	1.40E+03
IMAP[psia]	2.41E+01	2.63E+01	2.72E+01	2.83E+01	2.96E+01	3.11E+01
Inlet Air Temperature[C]	5.25E+01	5.33E+01	5.37E+01	5.39E+01	5.57E+01	5.59E+01
Intake Manifold Temp[C]	6.64E+01	7.20E+01	7.40E+01	7.56E+01	7.89E+01	8.04E+01
Boost Temp[C]	2.15E+02	2.17E+02	2.18E+02	2.18E+02	2.20E+02	2.24E+02
Inlet Air RH[%]	3.03E+01	3.03E+01	3.03E+01	3.03E+01	3.03E+01	3.03E+01
Exhaust Temp[C]	6.65E+02	6.33E+02	6.19E+02	6.08E+02	6.01E+02	5.90E+02
Turbine In Temp[C]	8.10E+02	7.76E+02	7.61E+02	7.50E+02	7.42E+02	7.32E+02
Exh Port 1[C]	7.61E+02	7.23E+02	7.08E+02	6.97E+02	6.88E+02	6.80E+02
Exh Port 2[C]	7.33E+02	6.98E+02	6.87E+02	6.76E+02	6.70E+02	6.63E+02
Exh Port 3[C]	7.35E+02	7.01E+02	6.91E+02	6.81E+02	6.73E+02	6.65E+02
Exh Port 4[C]	7.47E+02	7.11E+02	7.00E+02	6.90E+02	6.81E+02	6.73E+02
Exh Port 5[C]	7.68E+02	7.34E+02	7.22E+02	7.09E+02	7.01E+02	6.90E+02
Exh Port 6[C]	7.42E+02	7.10E+02	6.96E+02	6.84E+02	6.74E+02	6.65E+02
JW Out Temp[C]	6.26E+01	6.39E+01	6.43E+01	6.45E+01	6.66E+01	6.68E+01
ACW In Temp[C]	5.15E+01	5.40E+01	5.50E+01	5.58E+01	5.86E+01	5.90E+01
Dyno In Temp[C]	5.49E+01	5.83E+01	5.98E+01	6.10E+01	6.46E+01	6.51E+01
Dyno Out Temp[C]	6.31E+01	6.66E+01	6.82E+01	6.94E+01	7.29E+01	7.35E+01
Oil Sump Temp[C]	8.65E+01	9.03E+01	9.08E+01	9.10E+01	9.26E+01	9.25E+01
Oil Rifle Temp[C]	9.16E+01	9.65E+01	9.73E+01	9.75E+01	9.90E+01	9.89E+01
Oil Pressure[psig]	8.27E+01	8.07E+01	8.06E+01	8.06E+01	8.01E+01	8.03E+01
THC[ppm dry]	5.10E+02	5.10E+02	5.59E+02	6.25E+02	7.23E+02	9.69E+02
O2[%dry]	2.00E+00	4.21E+00	5.00E+00	5.78E+00	6.46E+00	7.14E+00
CO2[% dry]	1.05E+01	9.25E+00	8.77E+00	8.35E+00	7.95E+00	7.58E+00
CO[ppm dry]	6.43E+02	4.70E+02	5.31E+02	5.97E+02	6.47E+02	6.21E+02
Jacket Water Flow [gpm]	4.31E+02	4.32E+02	4.32E+02	4.32E+02	4.33E+02	4.34E+02
Intercooler Flow [gpm]	5.51E+02	5.50E+02	5.50E+02	5.49E+02	5.48E+02	5.47E+02
Dyno Water Flow [gpm]	1.64E+02	1.65E+02	1.65E+02	1.66E+02	1.66E+02	1.66E+02
Ambient Pressure[psia]	1.24E+01	1.24E+01	1.24E+01	1.24E+01	1.24E+01	1.24E+01
NO (350,3000) 191C	4.42E+03	3.44E+03	2.39E+03	1.39E+03	7.17E+02	3.16E+02
NO2 (150) 191C (1of2)	2.27E+01	5.96E+01	6.74E+01	7.54E+01	8.60E+01	8.04E+01
NO2 (2000) 191C (2of2)	2.21E+01	5.88E+01	6.68E+01	7.53E+01	8.67E+01	8.16E+01
N2O (100,200,300) 191C	9.11E-01	5.69E-01	4.02E-01	2.78E-01	1.83E-01	1.00E-01
NH3 (300) 191C (1of2)	7.02E-01	2.19E+00	4.27E+00	5.58E+00	4.35E+00	3.03E+00
NH3 (3000) 191C (2of2)	2.09E+00	3.96E+00	5.77E+00	6.43E+00	5.15E+00	3.89E+00
H2O% (25) 191C	1.83E+01	1.69E+01	1.61E+01	1.54E+01	1.52E+01	1.44E+01
CO2% (20) 191C (1of2) R4	9.02E+00	8.09E+00	7.78E+00	7.47E+00	7.15E+00	6.87E+00
CO (500) 191C (1of3)	4.50E+02	4.20E+02	4.73E+02	5.29E+02	5.75E+02	5.58E+02

CO% (1) 191C (2of3)	4.93E-02	4.08E-02	4.60E-02	5.20E-02	5.62E-02	5.48E-02
CH4 (3000) 191C (1of2)	2.92E+02	3.03E+02	3.46E+02	4.03E+02	4.84E+02	6.62E+02
CH4 (20000) 191C (2of2)	2.96E+02	3.09E+02	3.54E+02	4.08E+02	4.85E+02	6.57E+02
Ethane (500) 191C	1.39E+01	1.47E+01	1.69E+01	1.96E+01	2.28E+01	3.37E+01
Ethylene (100,3000) 191C	2.64E+01	2.24E+01	2.43E+01	2.76E+01	3.35E+01	4.47E+01
Acetylene (1000) 191C	6.59E+00	3.08E+00	2.62E+00	2.16E+00	2.03E+00	1.87E+00
Propane (200) 191C	3.46E+00	4.02E+00	3.52E+00	3.00E+00	1.80E+00	2.41E+00
Propylene (200,1000) 191C	4.09E-01	4.21E-01	5.27E-01	5.70E-01	7.73E-01	1.24E+00
Oil as octane (200) 191C	3.40E+00	4.09E+00	3.87E+00	3.40E+00	2.26E+00	2.07E+00
Formaldehyde (70,500) 191C	2.24E+01	2.43E+01	2.68E+01	2.99E+01	3.47E+01	4.34E+01
Acetaldehyde (1000) 191C	2.59E+00	3.18E+00	3.41E+00	3.53E+00	3.47E+00	3.98E+00
Formic Acid (100) 191C	4.38E-01	2.96E-01	2.87E-01	3.82E-01	6.23E-01	4.55E-01
MeOH (1000) 191C	2.44E+00	1.61E+00	1.61E+00	1.74E+00	1.79E+00	1.96E+00
CO% (10) 191C (3of3)	4.65E-02	3.84E-02	4.38E-02	5.14E-02	5.62E-02	5.32E-02
CO2 low% (4) 191C (2of2)	8.87E+00	8.05E+00	7.76E+00	7.46E+00	7.15E+00	6.89E+00
1,3 butadiene (80) 191C	2.86E-01	3.90E-01	3.94E-01	-1.23E-01	-4.32E-01	-7.84E-02
Temp (C)	1.91E+02	1.91E+02	1.91E+02	1.91E+02	1.91E+02	1.91E+02
Pressure (Atm)	9.80E-01	9.81E-01	9.81E-01	9.81E-01	9.80E-01	9.80E-01
NOx autorange	4.44E+03	3.50E+03	2.45E+03	1.47E+03	8.03E+02	3.96E+02
CO autorange	5.02E+02	4.20E+02	4.73E+02	5.29E+02	5.66E+02	5.54E+02
CH4 autorange	2.92E+02	3.03E+02	3.46E+02	4.03E+02	4.84E+02	6.62E+02
NH3 autorange	7.02E-01	2.19E+00	4.27E+00	5.58E+00	4.35E+00	3.03E+00
NOx autorange dry	5.43E+03	4.20E+03	2.92E+03	1.73E+03	9.47E+02	4.62E+02
CO autorange dry	6.14E+02	5.05E+02	5.63E+02	6.25E+02	6.67E+02	6.47E+02
CO2% autorange dry	1.10E+01	9.73E+00	9.28E+00	8.83E+00	8.43E+00	8.02E+00
N2O dry	1.12E+00	6.84E-01	4.79E-01	3.28E-01	2.16E-01	1.17E-01
NH3 autorange dry	8.60E-01	2.64E+00	5.09E+00	6.59E+00	5.12E+00	3.54E+00
FIDeq THC ppmC	4.26E+02	4.26E+02	4.79E+02	5.51E+02	6.55E+02	8.96E+02
FIDeq NMHC ppmC	1.05E+02	9.26E+01	9.84E+01	1.07E+02	1.22E+02	1.68E+02
FIDeq NMNEHC ppmC	7.74E+01	6.32E+01	6.46E+01	6.83E+01	7.62E+01	1.00E+02
CO2% autorange	9.02E+00	8.09E+00	7.78E+00	7.47E+00	7.15E+00	6.87E+00
FTIR NMHC ppmC	1.31E+02	1.20E+02	1.29E+02	1.41E+02	1.61E+02	2.17E+02
FTIR NMNEHC ppmC	1.03E+02	9.05E+01	9.47E+01	1.02E+02	1.16E+02	1.50E+02

APPENDIX D

Minute	449.46	451.42	454.46	457.43	460.42	463.47
Location	Outlet	Inlet	Outlet	Inlet	Outlet	Inlet
NO (350,3000) 191C	4700.325	4546.753	4704.662	4688.417	4701.257	4660.516
NO2 (150) 191C (1of2)	32.886	39.242	33.027	42.148	33.423	40.196
NO2 (2000) 191C (2of2)	32.192	38.249	32.598	41.124	33.291	39.117
N2O (100,200,300) 191C	2.543	0.645	2.066	0.759	1.660	0.746
NH3 (300) 191C (1of2)	0.429	0.563	0.473	0.414	0.408	0.329
NH3 (3000) 191C (2of2)	1.742	1.810	1.988	1.884	1.755	1.576
H2O% (25) 191C	17.454	19.569	17.301	17.232	17.224	17.381
CO2% (20) 191C (1of2) R4	9.066	8.733	9.089	8.989	9.082	9.017
CO (500) 191C (1of3)	305.039	230.698	420.147	241.343	495.989	237.353
CO% (1) 191C (2of3)	0.029	0.022	0.040	0.023	0.048	0.023
CH4 (3000) 191C (1of2)	-0.494	364.948	8.134	368.105	37.265	372.668
CH4 (20000) 191C (2of2)	11.984	367.872	20.170	377.239	49.964	379.580
Ethane (500) 191C	-0.483	22.326	-0.515	21.990	-0.544	22.315
Ethylene (100,3000) 191C	0.467	29.541	1.358	29.994	4.595	30.494
Acetylene (1000) 191C	1.834	4.062	2.481	4.352	2.924	4.378
Propane (200) 191C	-0.272	1.518	-0.234	1.320	-0.305	1.334
Propylene (200,1000) 191C	-0.454	0.500	-0.444	0.698	-0.475	0.621
Oil as octane (200) 191C	1.116	1.190	1.102	1.257	1.076	1.229
Formaldehyde (70,500) 191C	14.462	32.716	6.953	23.504	6.948	23.141
Acetaldehyde (1000) 191C	0.521	2.501	0.305	2.061	0.127	2.140
Formic Acid (100) 191C	0.260	0.316	0.245	0.187	0.219	0.178
MeOH (1000) 191C	0.733	2.039	0.450	2.030	0.548	2.169
CO% (10) 191C (3of3)	0.023	0.017	0.034	0.016	0.041	0.016
CO2 low% (4) 191C (2of2)	8.915	8.668	8.921	8.850	8.912	8.867
NOx autorange	4733.212	4585.995	4737.689	4730.565	4734.679	4700.712
CO autorange	305.039	230.698	420.147	241.343	495.967	237.353
CH4 autorange	-0.494	364.948	8.134	368.105	37.265	372.668
NH3 autorange	0.429	0.563	0.473	0.414	0.408	0.329
NOx autorange dry	5733.994	5701.815	5728.809	5715.408	5719.846	5689.612
CO autorange dry	369.618	286.822	508.185	291.583	599.200	287.285
CO2% autorange dry	10.984	10.857	10.990	10.861	10.971	10.914
N2O dry	3.080	0.801	2.498	0.917	2.004	0.903
NH3 autorange dry	0.519	0.699	0.572	0.500	0.493	0.398
FIDeq THC ppmC	1.670	517.955	14.486	522.278	53.381	528.784
FIDeq NMHC ppmC	2.214	116.512	5.538	117.363	12.390	118.849
FIDeq NMNEHC ppmC (VOC)	3.179	71.859	6.569	73.383	13.478	74.219
CO2% autorange	9.066	8.733	9.089	8.989	9.082	9.017
FTIR NMHC ppmC	16.913	152.987	12.264	144.447	19.324	145.727
FTIR NMNEHC ppmC	17.878	108.334	13.295	100.468	20.412	101.097

Minute	466.43	469.45	472.48	475.43	478.43	481.43
Location	Outlet	Inlet	Outlet	Inlet	Outlet	Inlet
NO (350,3000) 191C	4683.496	4663.519	4681.721	4672.570	4668.554	4590.785
NO2 (150) 191C (1of2)	35.027	40.622	37.298	40.815	39.315	36.609
NO2 (2000) 191C (2of2)	34.627	39.400	36.882	40.254	38.522	34.948
N2O (100,200,300) 191C	1.355	0.730	1.188	0.761	1.048	0.754
NH3 (300) 191C (1of2)	0.327	0.367	0.297	0.222	0.227	0.220
NH3 (3000) 191C (2of2)	1.862	1.547	1.902	1.385	1.945	1.586
H2O% (25) 191C	17.297	17.284	17.057	16.954	17.174	17.713
CO2% (20) 191C (1of2) R4	9.042	9.000	9.065	9.037	9.075	9.036
CO (500) 191C (1of3)	510.957	237.097	491.727	237.311	454.274	229.441
CO% (1) 191C (2of3)	0.049	0.023	0.047	0.023	0.044	0.022
CH4 (3000) 191C (1of2)	82.762	368.218	139.090	379.569	195.972	373.084
CH4 (20000) 191C (2of2)	94.411	378.154	153.159	388.755	208.238	380.983
Ethane (500) 191C	-0.568	21.905	0.008	22.659	1.083	22.177
Ethylene (100,3000) 191C	10.140	30.116	17.305	30.559	24.389	30.917
Acetylene (1000) 191C	3.424	4.321	3.257	4.566	3.988	4.498
Propane (200) 191C	-0.232	1.288	-0.395	1.321	-0.472	1.121
Propylene (200,1000) 191C	-0.545	0.609	-0.345	0.526	-0.324	0.660
Oil as octane (200) 191C	1.117	1.229	1.173	1.218	1.125	1.237
Formaldehyde (70,500) 191C	9.583	23.032	13.294	24.059	17.677	24.840
Acetaldehyde (1000) 191C	0.699	1.973	1.502	2.138	1.151	2.080
Formic Acid (100) 191C	0.226	0.225	0.198	0.181	0.229	0.219
MeOH (1000) 191C	0.652	1.968	0.644	2.071	0.716	2.095
CO% (10) 191C (3of3)	0.044	0.017	0.043	0.015	0.038	0.015
CO2 low% (4) 191C (2of2)	8.895	8.861	8.917	8.900	8.930	8.894
NOx autorange	4718.523	4704.141	4719.020	4713.384	4707.869	4627.394
CO autorange	510.884	237.097	491.716	237.311	454.273	229.441
CH4 autorange	82.762	368.218	139.090	379.569	195.972	373.084
NH3 autorange	0.327	0.367	0.297	0.222	0.227	0.220
NOx autorange dry	5705.436	5687.028	5689.480	5675.618	5684.141	5623.499
CO autorange dry	617.733	286.633	592.859	285.756	548.533	278.846
CO2% autorange dry	10.934	10.880	10.929	10.882	10.957	10.981
N2O dry	1.637	0.883	1.432	0.917	1.265	0.917
NH3 autorange dry	0.395	0.444	0.358	0.267	0.275	0.267
FIDeq THC ppmC	115.135	522.040	191.541	537.326	271.303	529.529
FIDeq NMHC ppmC	24.097	117.000	38.543	119.800	55.734	119.137
FIDeq NMNEHC ppmC (VOC)	25.233	73.189	38.526	74.482	53.568	74.782
CO2% autorange	9.042	9.000	9.065	9.037	9.075	9.036
FTIR NMHC ppmC	34.121	143.599	53.054	147.419	75.151	147.682
FTIR NMNEHC ppmC	35.257	99.789	53.037	102.101	72.985	103.327

Minute	484.45	487.46	490.46	493.56	496.46	499.55
Location	Outlet	Inlet	Outlet	Inlet	Outlet	Inlet
NO (350,3000) 191C	4594.743	4588.558	4575.676	4533.752	4584.635	4622.060
NO2 (150) 191C (1of2)	39.733	34.950	40.834	33.489	43.204	34.307
NO2 (2000) 191C (2of2)	38.546	33.597	39.946	32.328	43.361	34.156
N2O (100,200,300) 191C	0.932	0.791	0.903	0.736	0.883	0.769
NH3 (300) 191C (1of2)	0.292	0.318	0.250	0.310	0.209	0.178
NH3 (3000) 191C (2of2)	1.781	1.554	1.604	1.240	1.724	1.853
H2O% (25) 191C	17.736	17.484	17.453	18.251	17.304	16.858
CO2% (20) 191C (1of2) R4	9.047	9.088	9.103	8.997	9.135	9.171
CO (500) 191C (1of3)	394.108	228.196	350.572	224.727	320.416	229.168
CO% (1) 191C (2of3)	0.038	0.022	0.034	0.022	0.031	0.022
CH4 (3000) 191C (1of2)	241.656	376.405	278.876	372.181	306.979	387.294
CH4 (20000) 191C (2of2)	251.780	385.253	288.121	377.576	314.862	397.413
Ethane (500) 191C	3.079	22.691	5.730	22.741	8.559	23.903
Ethylene (100,3000) 191C	29.464	31.590	33.039	31.830	34.562	32.593
Acetylene (1000) 191C	4.073	4.612	4.340	4.550	4.307	4.803
Propane (200) 191C	-0.401	1.131	-0.289	1.324	-0.128	1.299
Propylene (200,1000) 191C	-0.106	0.728	0.087	0.661	0.326	0.547
Oil as octane (200) 191C	1.098	1.205	1.093	1.197	1.077	1.244
Formaldehyde (70,500) 191C	21.472	26.162	24.200	28.095	26.109	27.311
Acetaldehyde (1000) 191C	1.641	2.309	1.781	2.268	2.153	1.799
Formic Acid (100) 191C	0.260	0.229	0.270	0.280	0.268	0.232
MeOH (1000) 191C	0.766	2.135	0.829	2.161	0.982	2.163
CO% (10) 191C (3of3)	0.033	0.015	0.028	0.014	0.024	0.014
CO2 low% (4) 191C (2of2)	8.910	8.926	8.965	8.858	8.997	9.029
NOx autorange	4634.477	4623.508	4616.510	4567.242	4627.840	4656.367
CO autorange	394.108	228.196	350.572	224.727	320.416	229.168
CH4 autorange	241.656	376.405	278.876	372.181	306.979	387.294
NH3 autorange	0.292	0.318	0.250	0.310	0.209	0.178
NOx autorange dry	5633.386	5603.175	5592.640	5586.790	5596.300	5600.545
CO autorange dry	479.013	276.534	424.685	274.889	387.481	275.631
CO2% autorange dry	10.997	11.013	11.028	11.006	11.046	11.031
N2O dry	1.132	0.959	1.093	0.900	1.068	0.925
NH3 autorange dry	0.356	0.385	0.303	0.380	0.252	0.214
FIDeq THC ppmC	336.231	535.986	390.796	532.135	431.343	552.738
FIDeq NMHC ppmC	70.409	121.941	84.032	122.736	93.666	126.714
FIDeq NMNEHC ppmC (VOC)	64.250	76.559	72.572	77.254	76.549	78.909
CO2% autorange	9.047	9.088	9.103	8.997	9.135	9.171
FTIR NMHC ppmC	94.208	151.890	110.913	154.735	122.807	157.841
FTIR NMNEHC ppmC	88.050	106.508	99.453	109.253	105.690	110.035

Minute	502.48	505.48	508.48	511.53	514.13
Location	Outlet	Inlet	Outlet	Inlet	Outlet
NO (350,3000) 191C	4571.593	4529.131	4542.583	4585.307	4563.337
NO2 (150) 191C (1of2)	42.910	33.571	43.017	32.678	43.657
NO2 (2000) 191C (2of2)	43.239	33.000	43.362	32.268	43.855
N2O (100,200,300) 191C	0.858	0.774	0.827	0.771	0.829
NH3 (300) 191C (1of2)	0.133	0.084	0.199	0.179	0.155
NH3 (3000) 191C (2of2)	1.679	1.561	1.622	1.491	1.543
H2O% (25) 191C	17.180	17.547	17.531	16.809	17.302
CO2% (20) 191C (1of2) R4	9.168	9.101	9.133	9.191	9.146
CO (500) 191C (1of3)	292.208	222.276	276.418	223.904	264.964
CO% (1) 191C (2of3)	0.028	0.021	0.027	0.022	0.025
CH4 (3000) 191C (1of2)	327.953	389.203	348.073	390.009	358.357
CH4 (20000) 191C (2of2)	337.700	396.876	354.591	398.942	364.603
Ethane (500) 191C	11.541	24.234	14.226	24.038	16.078
Ethylene (100,3000) 191C	34.958	32.935	35.306	32.814	34.759
Acetylene (1000) 191C	4.463	4.778	4.527	4.902	4.470
Propane (200) 191C	0.114	1.505	0.402	1.281	0.511
Propylene (200,1000) 191C	0.483	0.517	0.596	0.676	0.586
Oil as octane (200) 191C	1.082	1.171	1.092	1.215	1.104
Formaldehyde (70,500) 191C	27.239	28.654	29.069	27.933	29.375
Acetaldehyde (1000) 191C	2.042	1.933	2.250	2.289	2.480
Formic Acid (100) 191C	0.237	0.261	0.252	0.221	0.243
MeOH (1000) 191C	1.211	2.293	1.491	2.293	1.602
CO% (10) 191C (3of3)	0.021	0.014	0.020	0.013	0.018
CO2 low% (4) 191C (2of2)	9.027	8.957	9.001	9.031	9.019
NOx autorange	4614.503	4562.702	4585.600	4617.986	4606.994
CO autorange	292.208	222.276	276.418	223.904	264.964
CH4 autorange	327.953	389.203	348.073	390.009	358.357
NH3 autorange	0.133	0.084	0.199	0.179	0.155
NOx autorange dry	5571.741	5533.712	5560.352	5551.009	5570.841
CO autorange dry	352.857	269.586	335.201	269.137	320.394
CO2% autorange dry	11.070	11.039	11.074	11.048	11.060
N2O dry	1.036	0.938	1.002	0.926	1.003
NH3 autorange dry	0.161	0.102	0.242	0.215	0.188
FIDeq THC ppmC	462.681	556.624	492.186	556.967	506.323
FIDeq NMHC ppmC	101.933	128.501	109.306	127.957	112.130
FIDeq NMNEHC ppmC (VOC)	78.851	80.033	80.853	79.880	79.974
CO2% autorange	9.168	9.101	9.133	9.191	9.146
FTIR NMHC ppmC	132.403	161.169	141.927	159.825	145.126
FTIR NMNEHC ppmC	109.321	112.700	113.474	111.748	112.970